ALMA MATER STUDIORUM – UNIVERSITÀ DI BOLOGNA

SCUOLA DI INGEGNERIA E ARCHITETTURA

DIPARTIMENTO di INGEGNERIA CIVILE, CHIMICA, AMBIENTALE E DEI MATERIALI DICAM

CORSO DI LAUREA MAGISTRALE in INGEGNERIA CHIMICA E DI PROCESSO

TESI DI LAUREA MAGISTRALE

in

Dinamica e Controllo dei Processi Chimici

MODELLING OF THE SEDIMENTATION PHENOMENON OF SOLID PARTICLES IMMERSED IN A TURBULENT FLUID

CANDIDATO:

Salvatore Evola

RELATORE:

Chiar.mo Prof. Alessandro Paglianti

CORRELATORI:

Prof. Giuseppina Montante

Dr. Claudio Pereira Da Fonte

Anno Accademico 2018/2019
Sessione III

Abstract

Settling phenomenon of solid particles immersed in a turbulent fluid has been investigated, in a condition of free-stream turbulence.

Since structures formed onto this condition are complex, it is difficult to predict exactly how particles move. It is thus appropriate to conduct deepen studies of the phenomenon and carry out simulations to describe particles' settling velocity.

In order to define a new correlation for the evaluation of particles' settling velocity, different literature correlations and parameters have been exploited.

Langevin dynamics has been used to describe fluid's motion, and by considering several forces acting on particles (buoyancy, drag, gravitational and virtual mass), it has been possible to evaluate their settling velocity, through a computational approach. Data have been obtained by varying characteristic properties, such as kinetic energy, its rate of dissipation, and physical properties of fluid and particles.

Aiming to find a reliable correlation which best explains the settling phenomenon, results in output from simulations have been compared with that deriving from proposed correlation. Encouraging results have been obtained over the range of operating conditions examined.

Table of Contents

Introduction

The modelling of sedimentation, suspension and fluidisation phenomenon of solid particles immersed in a turbulent fluid is of considerable importance for the chemical industry and environmental studies.

Settling behaviour of particles in turbulence flow can be found in various natural processes, such as suspended particles in the atmosphere, sedimentation in rivers and turbidity currents on the coast. It also occurs in much industrial equipment of, among others, pharmaceutical, food industry, chemical and biochemical reactor.

In the civil context, the study of dispersion and deposit of solid particles is used in designing some branches in sanitary systems useful for the treatment of drinking and purification water. While, common applications in environmental engineering aim to characterize the dispersion of particles, both in the atmosphere and in water bodies.

One more example of solid particles dispersion and sedimentation in the environmental field is linked to the disaster that recently occurred in the forests of Australia, where 25.5 million acres have burned, thus pouring numerous solid particles into the atmosphere through the wind. This is an effective example of solid particles immersed in a turbulent fluid, that allows comprising the extremely importance of correct prediction of particles motion.

The studying of settling phenomenon is widespread in chemical engineering; for this reason, it is a useful tool for investigating particles behaviour flowing into equipment applied in unit operations.

Types of equipment involve solid particles, in granules, used as raw materials and/or industrial solutions. Typical examples of applications in chemical industry may be the catalytic fluidized bed cracking present in the refinery, sedimentation tanks and crystallises for the separation of suspensions, fluid beds used as reactors to promote contact between phases, more generally in all processes with solid catalysts.

Since particles trajectory is influenced by turbulence flow, it is difficult to predict their exact path. Those random motion inspired many authors to conduct studies in this regard.

Turbulence was investigated experimentally since the end of the nineteenth century, thanks to Reynolds' researches. His experiment demonstrated the fundamental difference between the laminar and turbulent flow. Reynolds observed how the motion of the fluid was related to a dimensionless parameter, later to be known by its own name.

In 1921 the English physicist G.I. Taylor proposed the concept of homogeneous and isotropic turbulence, valid only in the free space, which represents an ideal case of turbulent flow in which the dynamics of fluid motion is neither influenced by interactions with tank walls nor by any average velocity field.

This concept has proved effective in the study of small turbulence scales, despite real turbulent flows are not homogeneous and isotropic.

The turbulent flow, due to the mixing of the fluid particles, is characterized by a high diffusivity and levels of vorticity. The structures that are formed in this regime are defined vortices (or eddies), and these tend to join and separate, to rotate and stretch.

L. Richardson in 1922 supposed the phenomenon of the cascade of energy, in which there are structures of different sizes, whereby non-linear interactions energy is transferred from the largest vortices to the gradually smaller ones, until the energy is dissipated by the effect of viscosity, as heat.

Kolmogorov in 1941 honed the idea of L. Richardson giving it a quantitative form. He supposed that the cascade transfer takes place through an energy flow that defines the average rate of dissipated kinetic energy.

The knowledge of turbulent flow and settling velocity of particles involves the study of forces acting on particles. It is important to underline that, referring to free-stream turbulence, drag coefficient contained into the equation of drag force doesn't have a clear mathematical expression.

For this reason, several experimental and computational studies were done to characterise the dynamics of particles in mechanically generated free-stream turbulence. However, there is still no universally accepted methodology that considers how random fluctuations of fluid phase influences solid particles.

Improving the fundamental knowledge of particle dynamics in turbulent flows is of considerable importance, for mainly, for the development of robust computational models for the design, optimisation and control of suspension and sedimentation processes.

This study proposes to analyse dynamics' particles in turbulent flow from a computational point of view and it has been developed thanks to a collaboration with the University of Manchester (UK).

An overview of main studies on the subject carried out by Spelt and Biesheuvel, Lane et al., Brucato et al. and Magelli et al. are presented in Chapter 1.

According to the current knowledge of the phenomenon, motivation and objectives of this study are explained in Chapter 2.

The underlying methodology of this project, described in Chapter 3, illustrates the principles used to carry out simulations and obtain experimental data.

In Chapter 4, a numerical model has been developed to simulate the trajectory of inertial particles in modelled turbulence, using Langevin dynamics, in § (3.2).

A sensitive analysis has been made under different conditions, in order to verify the assumptions, described in Chapter 3, and to obtain the most suitable conditions for the computational environment.

After this analysis, numerical simulations have been conducted to produce a data set of settling velocity.

A new correlation, based on analysed principles and results obtained, has been proposed to explain the settling velocity of solid particles in turbulent flows.

Eventually, project conclusions are presented in Chapter 5, while future works and exploitation purpose are illustrated in Chapter 6.

Chapter I – State of Art

1.1 Background

Since many types of equipment involved in process industry work with solid-fluid mixtures, understanding of how those two phases interact is of fundamental importance.

When a particle falls in a still fluid it is subject to a force called *Drag Force* (F_D), which acts in the direction of motion. Drag Force is a function of different factors, that for fluid at rest is expressed by the following relationship:

$$F_D = \frac{1}{2}\rho_f \, u_t{}^2 \, C_D \, A_p$$

(1.1)

where ρ_f is the fluid density, A_p is the area projected by the particle on a plane normal to the relative velocity u_t, and C_D is the Drag coefficient which is a dimensionless number that is determined experimentally.

When the fluid phase is at rest, or in laminar motion, a great deal of experimental information is available for many-particle shapes and physical situation, whether or not the relative motion between the two is able to induce turbulence in the fluid phase in the proximity of the particle. In such cases, a reliable estimate of the relevant C_D can be easily obtained [16].

An example of the relationship between the particles' Reynolds number (Re_p) and the experimental drag coefficients of spheres is shown in Fig. 1.
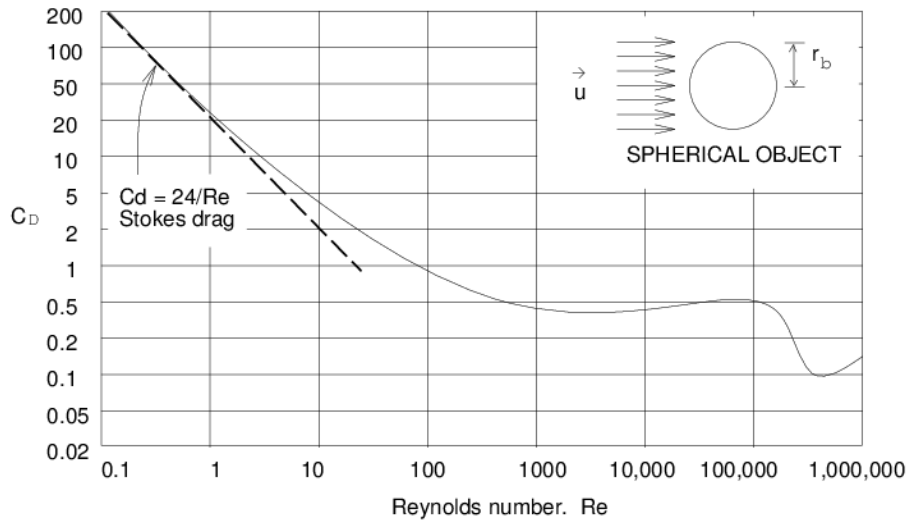
Fig. 1 – Plot of drag coefficient C_D against particles' Reynolds number for the fluid at rest.

In this case, the particle drag coefficient C_D depends only on the particles' Reynolds number:

$$Re_p = \frac{\rho\, u_t\, d_p}{\mu}$$
(1.2)

where ρ, d_p, μ are density, diameter and viscosity' particle, respectively.

With reference to a spherical particle, the continuity and momentum balance equation can be analytically solved leading to the well-known Stokes law, which can be put in the form [14]:

$$C_D = \frac{24}{Re_p}$$
(1.3)

That is not valid for higher Reynolds number, and drag coefficient referring to spherical shapes of the particle is correlated on a heuristic basis.

At Reynolds numbers around 1000, the drag coefficient begins to level off and stays approximately constant. This range is known as Newton region.

$$C_D = 0.44$$
(1.4)

When the Reynolds number increases between 10^5 and 10^6, the drag coefficient rapidly decreases and then increases again, due to the changing of boundary layer region which modifies the pressure distribution around the particle.

10

Solid particle falls in still fluid by means of the gravitational field, and it undergoes to three forces, like gravity, hydrostatic and drag. After a transient field, velocity becomes steady and the force balance can be written as:

$$C_D \frac{\pi d_p^2}{4} \frac{1}{2} \rho u_t^2 = \frac{\pi d_p^3}{4} (\rho_s - \rho) \qquad (1.5)$$

Where u_t is the terminal velocity, and it can be obtained from Eq.(1.6).

$$u_t = \left(\frac{4 g d_p \ (\rho_s - \rho)}{3 \ \rho \ C_D} \right)^{1/2} \qquad (1.6)$$

However, many situations involving free-stream turbulence, which can be generated by various sources. In this case, the particle drag coefficient C_D could be widely different with respect to the case of fluid at rest.

Free-stream turbulence refers to a system, like stirred reactors, where the presence of non-organised structures, as eddies, influences unpredictably fluid motion, therefore particles motion is complex to study.

Unfortunately, relative few data are available on the effect of free-stream turbulence on particle drag coefficients, especially for the particle sizes typically involved in the equipment of process industry [14].

Several studies on the calculation of drag coefficient have been addressed over the years, and they have briefly reported through the next paragraphs.

Most of them considered the hypothesis of homogeneous isotropic turbulence introduced by Taylor, thus they demonstrated that the settling velocity of heavy particles is enhanced by turbulence, due to the preferential sweeping phenomenon of particles along pathways between vortices.

The fluid dynamics of multiphase stirred equipment is complex, and the effective particle settling velocity in diluted suspension was shown to be smaller than that in a still liquid [2].

Bec et al. investigated the effect of gravity stemming from the density difference between particles and fluids on the settling velocity and clustering behaviour of particles in turbulence, by Direct Numerical Simulation (DNS). This study confirmed the acceleration

effect of particle inertia on the settling velocity and showed that the effect depends on the Stokes number and the Froude number [1].

Yang and Lei studied the behaviour of preferential sweeping in the low vorticity region, condition of homogeneous isotropic turbulent flows. They pointed out that preferential sweeping is controlled by small scales, as stated by Kolmogorov' hypothesis (reported in §1.4), but large turbulent scales also affect the increasing movement of the settling particles. This study showed that the flow vorticity is minimized when the Stokes number is close to one, which corresponds to the maximum increase in the settling velocity [11].

Zhou and Cheng studied the falling in the turbulence of a single large-sized particle of a density slightly heavier than water. They found that the settling velocity cannot be related to turbulence intensity or to the Stokes number. However, the drag coefficient of particles coming out from their experiments is significantly larger than the standard values; this might lead to a decrease in settling velocity. The small particle density differences from the carrier fluid might also play an important role in this reduction [4].

Magelli et al. [12] and *Brucato et. al* [3] have carried out studies taking into account the parameter d_p/λ. *Brucato et al.* obtained a direct measurement to calculate the drag coefficient, while *Magelli et al.* evaluated an average settling velocity by fitting the model predictions to experimental data.

Spelt and Biesheuvel proposed an analysis using a dimensionless parameter β, that is the ratio between the turbulence intensity and the rise velocity of the bubbles in still fluid. After studying the phenomenon for bubbles, they extended those case to that of particles, showing how the β value affects the settling rate of them [2].

Lane et al. [7] initially proposed a correlation involving Stokes number to explain turbulence effects on drag coefficient, by using available literature data. After some years, they noticed that the phenomenon is better explained also with the Richardson number.

This study is based on the analysis conducted by *Spelt and Biesheuvel (1997)*, *Brucato et al. (1998), Lane et al. (2007), Magelli et al. (2008)*, that investigated the behaviour of solid particles immersed in a fluid in free-stream turbulence.

Those studies are briefly reported in the following sections.

1.2 Previous studies conducted

1.2.1 Spelt and Biesheuvel (1997)

Spelt and Biesheuvel initially presented results of approximate analyses and numerical simulations of gas bubbles motion. After that, they adapted their previous study to that one related to solid particles motion, considering high Reynolds number under the hypothesis of homogeneous isotropic turbulence.

In order to simulate turbulent self-diffusion, settling and dispersion of small rigid particles, studies were conducted involving many Fourier modes varying randomly in space and time.

The forces exerted by the surrounding fluid on a settling particle are described by supposing that it acts on a rigid sphere in an inviscid unsteady non-uniform rotational flow *(Auton, Hunt & Prud'homme 1988)*. This drag force lead particle to settling steadily at high values of Reynolds number in still fluid; a good approximation for drag force can be obtained by calculation based on viscous potential flow theory (Moore 1963).

In these conditions, the dominant contribution to the statistics of the particle motion is associated to the autocorrelation function, with considering low-intensity turbulence and characteristics length scales of the same order of magnitude as those used for velocity relaxation of the particles.

They have found a satisfactory agreement between the analyses and the simulations, with a small value of the ratio between the turbulence intensity (u_0) and the settling velocity of the particles in still fluid, β (Eq. (1.9)).

For larger values of β it is conceivable that the instantaneous small-scale vorticity structure will become more important for statistics' particle motion, where it is governed by acceleration reaction forces.

Spelt and Biesheuvel used the Eq.(1.7) proposed by Thomas et al. (1984), that combines the expression of motion of small particles immersed in liquid, subjected to forces acting in an unsteady inviscid rotational flow, with that one typical of the drag force.

$$\frac{dV}{dt} = 3\frac{DU}{Dt} - (V - U) \times \Omega - 2g - \frac{1}{\tau_b}(V - U)$$

(1.7)

Where V is the particle's velocity, U is the fluid velocity, determined by Direct Numerical Simulations (DNS). $\Omega = \nabla \times U$ is the vorticity, while time constant τ_b is:

$$\tau_b = \frac{a^2}{18\nu} = \frac{V_T}{2g}$$

(1.8)

where a denoting the equivalent particles radius.

Various dimensionless parameters were used to characterise the motion of the particles.

$$\beta = \frac{u_0}{V_T}$$

(1.9)

$$\mu^* = \frac{L_{11}}{\tau_b V_T}$$

(1.10)

$$\lambda^* = \frac{\lambda}{\tau_b V_T}$$

(1.11)

μ^* relates the relaxation time τ_b of the particle to the characteristic time scales of turbulence. The integral length scale L_{11} is a measure of the size of eddies in the flow, and thus of the spatial variation of the turbulence.

λ^* relates the Kolmogorov scale of dissipative eddies (λ), with the integral time scale T_L, which is a measure of time variation of turbulence, and with relaxation time τ_b.

They used a grid turbulence $T_L/(L_{11}/u_0)$ approximately constant, without considering T_L/τ_b as an independent group*. It was specifically examined the case in which turbulent intensity is less than the particle settling velocity, i.e. $\beta \ll 1$. An increasing of β leads to an increase in settling velocity, thus particles drift easily through eddies. The group considered, λ^*, was used to compared different energy spectrum functions, as showed in Fig. 2.

By varying β, through variation of u_0, changes in turbulence' structure were studied, with fixed values of μ^*, λ^*, or both.
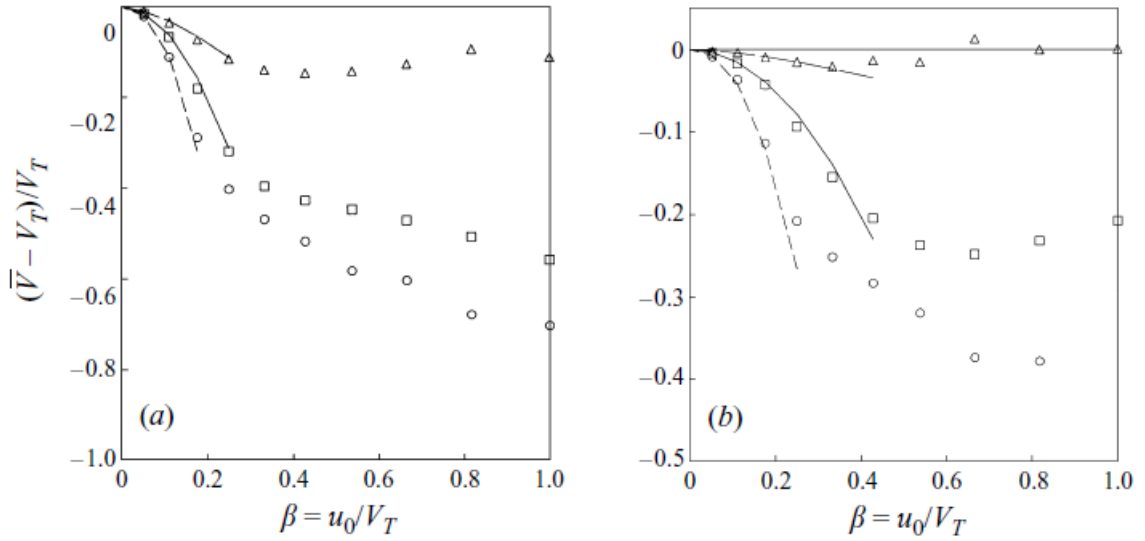
Fig. 2 – The difference between the mean velocity of the rise of a particle $\bar{V}$ in isotropic turbulence and its value in still fluid V_T, as a function of β. (a) □,——, Kraichnan spectrum with $\lambda^* = 1$ and $\mu *= (\pi/2)^{1/2}$; Δ,—— ——, von Karman-Pao spectrum with fixed Taylor microscale ($\lambda^* = 1$); ○,- - - -, von Karman-Pao spectrum with fixed integral scale ($\mu *= (\pi/2)^{1/2}$). (b) As in (a) but with $\lambda^* = 4$ and $\mu = 2(2\pi)^{1/2}$ Curves show the analytical results for small β. [9]

A higher value of the dimensionless group T_L/τ_b indicates whether the particles quickly respond to the turbulent velocity fluctuations.

In order to determinate correlation functions, fixed values for particles velocity and other parameters were considered. Simulations were carried out by involving a single particle released with a certain value of V_T, valid for a still fluid, with its trajectory calculated by a fourth-order version of the Bulirsch-Stoer scheme (Press et al. 1991) over a sufficiently long time, typically equal to $L_{11} = u_0$.

Referring to the case of free-stream turbulence, that takes place when β increases its value from 0 to 1, the deviation of mean settling velocity V_S, from its value in still fluid decreases up to 50%, due to an increase of turbulence intensity.

Therefore, from Fig. 2, it is possible to conclude that mean particle velocity gets lower with increasing turbulence intensity, in the range of $\beta = 0.3 \div 0.5$. For higher values of turbulence intensity, the particle velocity increases again or becomes approximately independent of β.

15

1.2.2 Lane et al. (2004 - 2007)

G.L. Lane et al. (2004) developed a correlation relating the drag coefficient to fluid turbulence characteristics through dimensionless Stokes number. They studied the effects of dispersed phase density and size on the applied drag force under turbulent conditions, extending the much-needed experiment data on particle drag coefficient in free-stream turbulence, as a function of solid particle's characteristics [6].

Due to the limitation of existing correlations, Lane et al. decided to make use of available literature data to develop another correlation. Using *Spelt and Biesheuvel* dimensionless groups (Eq. (1.9), Eq. (1.10)), combining these two parameters and taking into account that in isotropic turbulence one can relate the integral length scale, L_{11}, to the integral time scale, T_L , as $L_{11} = T_L \, u_0$, it was possible to write:

$$\frac{\beta}{\mu^*} = \frac{u_0}{V_T} \frac{L_{11}}{\tau_b V_T} = \frac{\tau_p}{T_L} \tag{1.12}$$

τ_p is the particle relaxation time and T_L is defined as $T_L = L/u_0$, where L is the integral length scale, and u_0 is the r.m.s. (root mean square) the velocity of turbulence.

The relaxation time of particles τ_p is given by:

$$\tau_p = \frac{\frac{\rho_p}{\rho_f} + C_A}{\left(\frac{3}{4}\right)\left(\frac{\overline{C_D}}{d_p}\right) U_T} \tag{1.13}$$

where $\overline{C_D}$ is the normalised drag coefficient, ρ_p, ρ_f, are particle and fluid density, respectively, and d_p is the particle size. C_A is the added mass coefficient equal to 0.5 [6].

The resulting parameter is Stokes number, that is a measure of the time taken for a particle to respond to an interacting turbulent eddy, and hence defined as:

$$St = \frac{\tau_p}{T_L} \tag{1.14}$$

The data from various sources were re-analysed and plotted as the ratio of turbulent to stagnant terminal velocity, correlating them with the Stokes number, as it is possible to see in Fig. 3.

Although available data indicate a continual decrease in slip velocity with increasing τ_p/T_L, further consideration must be given to how the relationship extrapolates to higher values. If the ratio becomes very large, this means that either the particle has a very large relaxation time, or the time scale of the turbulence is much shorter than that of the particle. In such cases, the particle does not respond to turbulence. Therefore, the curve must have a minimum somewhere, and beyond that minimum, the effect diminishes, so as $\tau_p/T_L \rightarrow \infty$, $U_s/U_t \rightarrow 1$ [7].
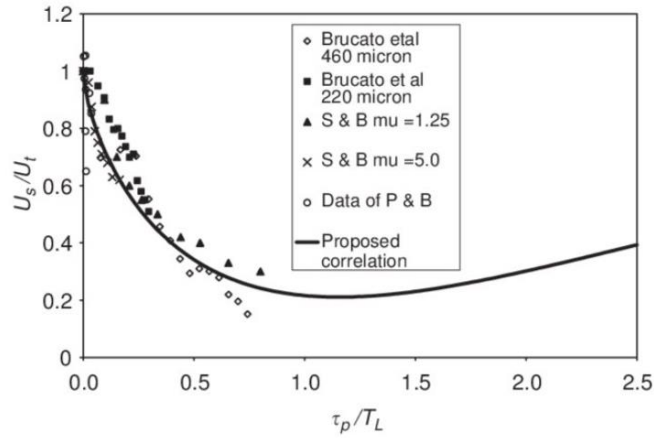
Fig. 3 – Literature data for U_s/U_t plotted against τ_p/T_L for solid particles and bubbles, with fitted correlation for a bubble as used in the CFD model [11].

As it can be seen from Fig.3, this correlation is valid only for Stokes numbers up to 0.7. By using CFD simulations, Lane et al. proposed a possible trend of the full curve; however, the precise shape remains uncertain [7].

Lane et al. correlation proposed is reported below.

$$\frac{U_s}{U_t} = 1 - 1.4\, St^{0.7} \exp(-0.6\, St) \qquad (1.15)$$

This is expressed in terms of $\overline{C_D}/C_{D_o}$, according to:

$$\frac{\overline{C_D}}{C_{D_o}} = \left(\frac{U_s}{U_t}\right)^{-2}$$

(1.16)

With C_{D_o} drag coefficient valid for still liquid.

Correlation proposed by Lane et al. captured the continual decrease in settling velocity of solid phase as Stokes number increases. When either the particle has large relaxation time or the time scale of turbulence is much shorter than that of the particle, the effect of the turbulence is considered to be negligible (i.e. as $\tau_p/T_L \to \infty$, $U_s/U_t \to 1$). This means that there will be a minimum in the plot corresponding to a maximum interaction between turbulence and particles [6].

In 2008 Lane et al. reviewed their previous work, dating it on how turbulence influences drag on particles, highlighting two points. Firstly, there was a clear advantage in using a stationary turbulence generator to eliminate any net mean flow effects; secondly, the dimensionless drag turbulence relationship proposed required experimental confirmation at higher Stokes numbers.

Studies were carried out to extend the experimental data on particle drag coefficients in free-stream turbulence, as a function of solid particles characteristics; in particular, the motion of different size particles made of Nylon and Teflon were examined in two different turbulent low fields, as shown in Fig.4.
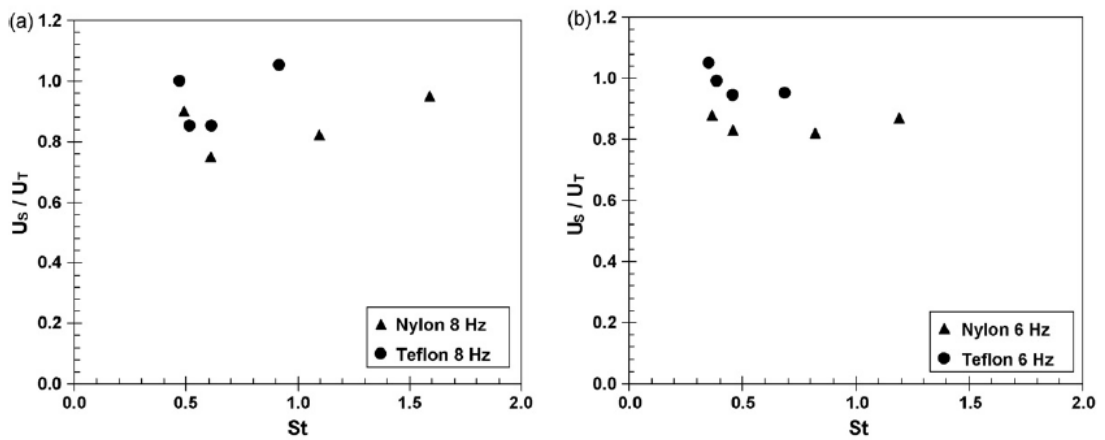

Fig. 4 – Effect of turbulence on the settling velocity of Nylon and Teflon particles generated at oscillating frequencies of (a) 8Hz and (b) 6Hz which corresponded to r.m.s. turbulence velocities of 19.2 and 14.4 mm/s, respectively. [8]

The results showed that the free-stream turbulence may lead to a significant reduction in settling velocity of solid particles, the function of particle characteristics as size and density.

As Stokes number increases, U_s/U_t reduces, as it can be seen also from raising in particles' diameter.

For higher Stokes numbers, and for particle's diameter greater than the integral length scale of turbulence, the ratio of velocity tends to return to values around unity, for both materials. This trend is probably related to the fact that no turbulent eddies of enough size or energy deflect the particle from its path.

There was a considerable discrepancy between Lane's correlation and the new experimental data obtained, as shown in Fig. 5(a).

Considering the correlation related to Lane et al. first study, new experiments carried out suggested that besides St number, both d_p/L and u_0/U_t ratios needed to be considered as separate entities in developing a correlation for particle drag coefficient in turbulent flows.
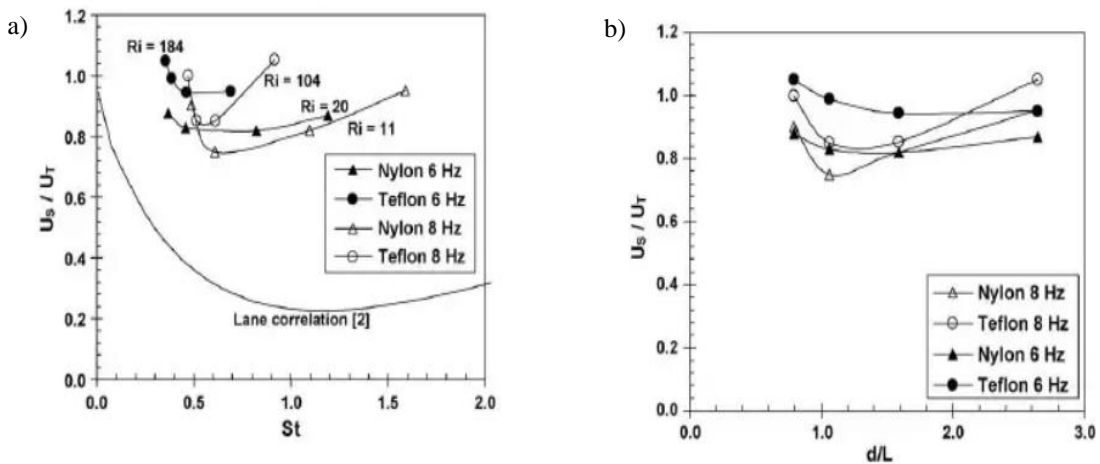
Fig. 5 – (a) Comparing the experiment data for settling velocity of solid particles in turbulent flows with the model prediction of Lane et al. [11]. The results are presented as a function of Stokes and Richardson numbers. (b) The effect of particle size relative to the integral length scale of turbulence on the particle settling velocity [8].

Fig. 5(b) suggests that the velocity curve starts to flatten as d_p/L reach the value of one. This behaviour was found to be irrespective of the particle density or turbulence intensity. Furthermore, in Fig. 5(b), it seemed that minimum value, $(U_s/U_t)_{min}$, for U_s/U_t occurred around $d_p/L = 1$ for all experimental tests.

The most probable reason is that the maximum interaction between the particle and the turbulent vortices occur when particle size is approximately equal to the turbulence integral length scale.

Authors suggested that inertial force due to turbulence, and the net effective weight of the particles, due to the gravity, play a key role in describing the dimensionless ratio between velocities. For this reason, was defined as a parameter called Richardson number.

$$Ri = \frac{g \left| \rho_p - \rho_f \right| L}{\rho_f \, u_0{}^2}$$

(1.17)

As shown in Fig. 6, a low value of Richardson number reflects the turbulence dominance. When Richardson number increases, the effect of turbulence on the settling velocity of particles reduces to negligible levels. Conversely, there appears to be a major effect on $(U_s/U_t)_{min}$ for low values of the Richardson number.
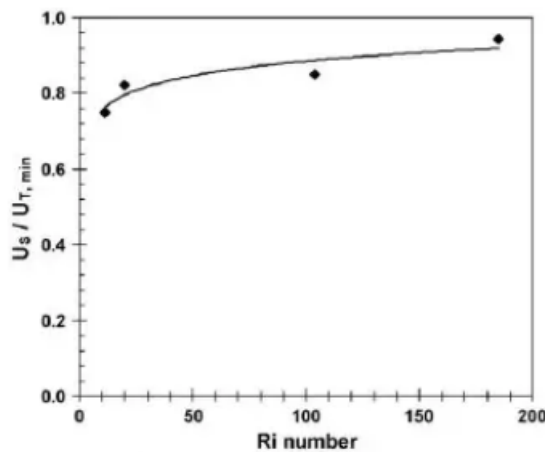
Fig. 6 – The maximum interaction between solid particles and turbulent eddies as a function of the Richardson number [8].

Concluding, particle density and turbulent intensity are the key parameters affecting the settling velocity, and from this, Richardson number is used to correlate the minimum reduction in the ratio between settling and terminal velocity, $(U_s/U_t)_{min}$.

1.2.3 Brucato et al. (1998) - Magelli et al. (2008)

Brucato et al. and *Magelli et al.* studied the behaviour of solid particles in the agitated system, by proposing a correlation to calculate the effective settling velocity.

Initially, Magelli et al. (1990) proposed a correlation suggesting that the influence of turbulence on particle settling velocity, expressed in terms of the ratio between the settling velocity in the turbulent medium and that in still liquid, was a function of the ratio between particle diameter (d_p) and Kolmogorov scale of dissipative eddies (λ). The latter is expressed by:

$$\lambda = \left(\frac{\nu^3}{\varepsilon}\right)^{1/4} \qquad (1.18)$$

where ε is the rate of kinetic energy dissipated per unit mass of fluid phase.

Data obtained from Magelli et al. study were gathered to indicating that the correlating parameter λ/d_p is related to the behaviour of the system. Unfortunately, those results did not fit well setting data used for the experiment, especially for the smallest glass beads, as it can be seen from Fig 7.
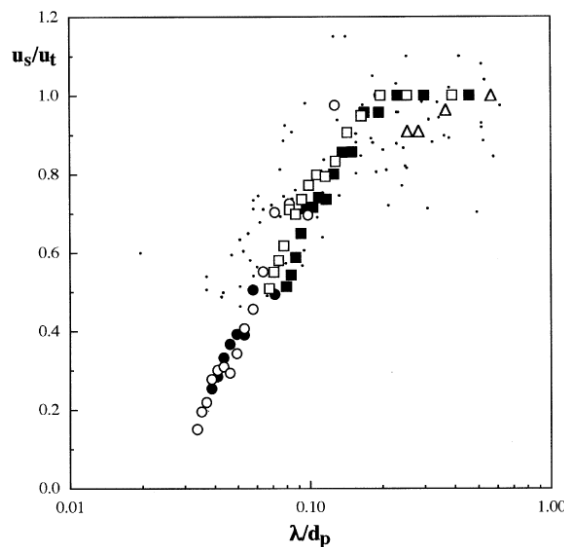

Fig. 7 – Comparison of experimental data with Magelli et al. (1990) experimental data (dots) and correlation. Glass beads (Δ) 63-71 μm, (□) 212-250 μm, (○) 425-500 μm, silica (▪) 180-212 μm, (●) 425-500 μm. [1]

21

Correlation proposed by Brucato et al. (1998) taken into consideration the reverse ratio proposed by Magelli et al. (1990) (i.e. d_p/λ). This term was directly correlated to the normalized drag coefficient (C_D) by a simple cube law.

$$\frac{C_\mathcal{D} - C_{\mathcal{D}_o}}{C_{\mathcal{D}_o}} = 8.76 \times 10^{-4} \left(\frac{d_p}{\lambda}\right)^3 \tag{1.19}$$

Subsequently, studies by Magelli et al. were based on the measurement of vertical solid concentration profiles at steady-state conditions, as well as of local concentration transients, and interpreting the data with a simple phenomenological model along the same lines followed in the past with settling solids from Nocentini et al. and Pinelli et al., and the particles settling velocity was determined.

The study was performed in a high aspect ratio vessel agitated with multiple impellers; this configuration allows to magnify the vertical concentration gradients, and thus to make the analysis more reliable [8].

The solids distribution was usually characterised by limited radial concentration gradient; consequently, the vertical concentration profiles are their main distinctive feature, so this distribution in the stirred vessel was interpreted with a simple one-dimensional model.

Using particles with density higher than the density of the fluid, by using non-dimensional coordinates for axis directed upwards, the dimensionless concentration under unsteady conditions, after an instantaneous injection at the base of the vessel, was calculated from a relationship, reported below.

$$C^*(\zeta, \theta) = f(Pe_s, \zeta) \tag{1.20}$$

$$C^* = C/C_{avg} \qquad\qquad Pe_s = U_s H/D_{es} \qquad\qquad \theta = tD_{es}/H^2$$

Where C^*, the dimensionless concentration, is a function of Pe_s and ζ. D_{es} is the dispersion coefficient and Pe_s is the Peclet number for the solids: its value is positive for the buoyant particles. ζ is the dimensionless coordinate, while H is vessel weight, and θ is the dimensionless time.

The particle rising velocity in the stirred tank was calculated from Pe_s and dispersion coefficient for the solid phase, considered equal to that for liquid phase, under steady-state measurement, $U_s = Pe_s D_{es}/H$. This was compared with terminal velocity (U_t), calculate with the Turton and Levenspiel's correlation.

Settling velocity was found significantly lower than terminal velocity, as the influence of the turbulence on particle settling velocity was related to particles diameter (d_p) and Kolmogorov scale of dissipative eddies (λ).

The values of the ratio U_s/U_t of Magelli et al. obtained, were compared with empirical correlation established for solid settling in a dilute, turbulent medium, as stated by Pinelli et al. (2001) and showed in Eq. (1.21).

$$\frac{Us}{Ut} = 0.4 \cdot tanh\left[16\frac{\lambda}{d_p} - 1\right] + 0.6 \qquad (1.21)$$

With the Kolmogorov scale of dissipative eddies (λ) given by the equation mentioned above.

Studying the effects of particle inertia under conditions of isotropic turbulence, and by analysing bubble gas motion in a turbulent medium *Oesterlè and Zaichik (2006), Doroodchi et al. (2008), Porte and Biesheuvel (2002)* suggested considering particle-fluid interaction, in particular related to solid-to-liquid density.

Afterwards, studies carried out by Scargiali (2007) shown that introducing ratio between solid and fluid density reduced the average error of about 20% of the previous correlation (Eq. 1.22). The optimal exponent value for this ratio is equal to 0.5.

$$\frac{Us}{Ut} = 0.32 \cdot tanh\left[19\frac{\lambda}{d_p}\left(\frac{\rho s - \rho f}{\rho f}\right)^{0.5} - 1\right] + 0.6 \qquad (1.22)$$

Eventually, *Magelli et al. (2008)* proposed a correlation to calculate U_s/U_t, which contain these two dimensionless parameters.

This correlation predicts solid distribution in processes where floating particles are dispersed in fluid, but it is possible to apply it also to describe gas-liquid systems, under idealised condition.
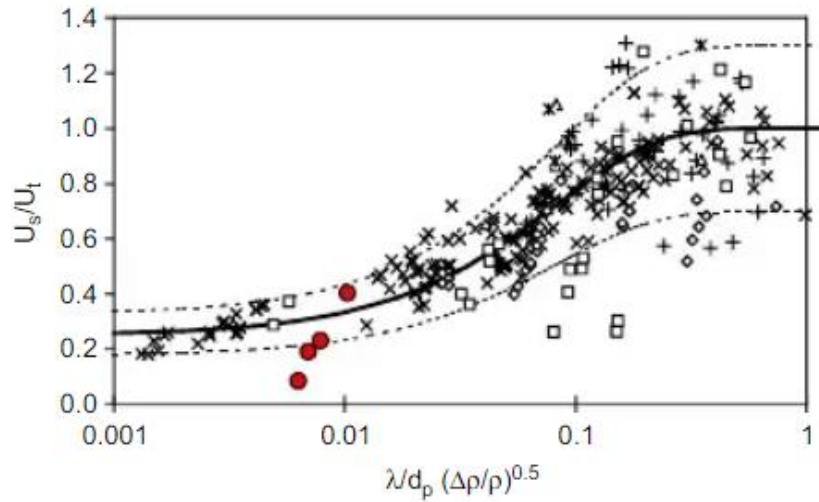
Eq. (1.22) is plotted in Fig. 8.

Fig. 8 – The ratio of the settling/rising velocity, U_s, in stirred systems to the terminal value, U_t, •; buoyant particles; other data points: settling particles (+××·; Rushton turbines of three scales; ◊Δ; PBT of two scales; □: A310 impellers) solid line: correlation for settling solids; dashed lines: ±30% of the correlation line. [2]

According to Brucato et al. studies, one can see that as dimensionless terms on abscissa for the lowest and highest values date not converge. The ratio of the velocity U_s/U_t reaches a unitary value, as shown by the typical behaviour of a fluid at rest.

1.3 Analysis of correlations

The analysis performed by different authors underlines the limitations in their proposed correlations. In order to improve knowledge of the phenomenon, further studies should be necessary.

Spelt and Biesheuvel based their studies on investigating particles motion of equivalent diameter of about 1,0 mm, in isotropic turbulent flow and their data just covered range of $\beta \ll 1$. Therefore, the applicability of the correlation of Spelt and Biesheuvel is questionable for the turbulence of high intensity at small length scales.

Lane et al. in their studies considered Spelt and Biesheuvel dimensionless parameter β and μ^*, and combining both they obtained Stokes number.

Correlation proposed initially by Lane et al. was valid for $St < 0.7$. By increasing Stokes number and particle diameter, U_s/U_t ratio decreases, reaching a minimum value for d_p/L equal to one, corresponding to a maximum interaction between turbulence and particles. The U_s/U_t increases as the Stokes number increase as well, returning to a unity value at ratios d_p/L of more than 2.5.

Lane et al. intuited that the difference in density between fluid and particle was an important parameter in describing settling velocity. They used this parameter, through Richardson number, in order to establish the greatest contribution between gravity force domains respect to turbulence.

Magelli et al., according to Brucato et al., proposed a correlation by using a dimensionless parameter, λ/d_p. Unfortunately, the highest value of this reached a U_s/U_t unitary, as shown by the typical behaviour of a fluid at rest.

In a second moment, Magelli et al. compared data with that of Pinelli et al., by concluding that the difference between particle and fluid density must be included in their correlation, with uncertainties regarding errors in measurement.

As suggested by Lane et al., the dimensionless parameters introduced by various authors should be considered as separate entities, in order to establish the exact relationship between them and particle settling velocity.

1.4 Kolmogorov Hypothesis

The first hypothesis that the disturbances in small scales in a turbulent fluid are approximately isotropic was found in the literature (*Richardson in 1922),* considering turbulence constituted by a set of disordered disturbances (eddies) that differ from each other in terms of size and scale.

Kolmogorov in 1941 stated that in the turbulent flow perturbations are characterized by the size of the vortex, and although it is a conceptual abstraction, its utility has greatly simplified the theoretical treatment and allows a better understanding of physics.

The energy terms involved in the motion of the fluid are characterized by instability mechanisms, that is the generation of vortices that over time generate ever-smaller vortices until the dimensions are not so small that the viscosity dissipates the structures preventing any further transfer.

Kolmogorov's hypothesis draws from the observation that the dynamics of turbulence depends on how quickly the energy is transferred from the large to the small scales and on the value of the viscosity that sets the wave number, to which the cut is made in the transfer of power. If the fluid dynamics phenomenon is statistically stationary, being the cascade from non-viscous energy, it is deduced that called the rate of turbulent kinetic energy (per unit of mass), (ε) produced in the unit of time transferred to the disturbances on a larger scale L, this will also be the energy dissipated in the unit of time.

Consequently, ε will be the characteristic of large scale of motions which will influence the statistical state of small scales fluctuations. The energy associated with them is of the order of u^2 and that the rate of kinetic energy dissipated will be $\varepsilon \sim v_L{}^3/L$, where v_L is the characteristic velocity related to a larger scale. At high Reynolds numbers, the direct dissipation of energy by the medium motion of the fluid under the action of the molecular viscosity is negligible, therefore the components of the instantaneous motion with relative fluctuations are considered:

$$\varepsilon = \frac{1}{2} \nu \sum_{i,j} \overline{\left(\frac{\partial u_\iota}{\partial x_j} + \frac{\partial u_j}{\partial x_\iota} \right)} \qquad (1.23)$$

u_i and u_j are the components of the instantaneous motion, in the direction i and j.

Kolmogorov claims that all the geometric information of the large vortices, determined by the average motion of the fluid, is lost. Consequently, the characteristics of small-scale motions must in a certain sense be universal, that is, similar for each high Reynolds number motion.

Considering the disturbances that have lost the directional property (anisotropy) of the average motion and are substantially isotropic, these will still have considerable dimensions and will have a characteristic size of the order of L. The description is given by *Pope (2003)*, for the length of the scale L_E (of the order of $1/6\ L$), was useful as a demarcation between the surely anisotropic vortices ($r < L_E$) and the small locally isotropic vortices ($r < L_E$).

The properties of large-scale motions can influence the statistical properties of lower-scale disturbances only through the turbulent energy dissipation rate ε.

Furthermore, these properties must also depend on the parameters that characterize the physical properties of the fluid, which can be described by the density ρ and the viscosity ν. Since, however, the relative speed values are independent of the choice of the mass unit, the statistical properties of the motion of the disturbances cannot depend on ρ.

We can conclude that the statistical properties of disturbances on a sufficiently small scale will depend only on ε and ν.

Kolmogorov's first hypothesis:

In the case of disturbances in a sufficiently high Reynolds number field of motion, the probability distribution for velocities in a region of space-time where turbulence is locally isotropic is defined unambiguously by the values of ε and ν.

Using variables such as the energy that dissolves (ε) and the viscosity that dissipates (ν), length scale is constructed dimensionally λ, that is the magnitudes of these vortices, and the corresponding velocity and time τ_λ of these vortices, as:

$$v_\lambda = (v\,\varepsilon)^{1/4} \qquad\qquad (1.24)$$

$$\lambda = \left(\frac{v^3}{\varepsilon}\right)^{1/4} \qquad\qquad (1.18)$$

$$\tau_\lambda = \left(\frac{v}{\varepsilon}\right)^{1/2} \qquad\qquad (1.25)$$

With this observation we can understand Kolmogorov's first hypothesis which says:

For sufficiently high Reynolds numbers, the characteristics of the small scales of all turbulent flows are universal and are determined by the viscosity and power dissipated.

To quantify the dissipation scales was defined the Kolmogorov scales, that is the size, velocity and time, we define a Reynolds number equal to:

$$Re = \frac{v_\lambda\,\lambda}{v} = 1 \qquad\qquad (1.26)$$

Disturbances with a length of λ scale, characterized by a velocity v_λ, have a number of Reynolds equal to $Re = v_\lambda\,\lambda\,/v\ = 1$. λ is of the same order of magnitude as the scale length of higher-order disturbances on which viscosity still has an appreciable effect. Using the definition of λ it is possible to identify a dimensional range for the disturbances within which their main characteristic is local isotropy, in fact, all the disturbances with scale length r lower than L and higher than Lam are locally isotropic.

The range $\lambda - L_E$ is called: <u>Universal Equilibrium Range</u>.

Now consider the ratio between the scale length of the smallest motions λ and the scale length of the vertices of larger dimensions L and the analogous ratios for the scale velocity and the characteristic scale time. These ratios are immediately determined by the definition of the Kolmogorov scale and by the fact that $\varepsilon \sim U^3/L$ in the following way:

$$\frac{\lambda}{L} = Re^{-3/4} \qquad\qquad (1.27)$$

$$\frac{v_\lambda}{U} = Re^{-1/4} \qquad\qquad (1.28)$$

$$\frac{\tau_\lambda}{T_L} = Re^{-1/2} \qquad\qquad (1.29)$$

Hence, the Kolmogorov length decreases with increasing Reynolds number which characterizes the motion of the fluid and as well as the scaling speed and the scaling time, but more slowly. Therefore, at high *Re* values, the velocity and the characteristic time of scale of the smaller vortices (v_λ and τ_λ) are small when compared with those of the larger vortices (U, T_L).

In the case in which the *Re* value of the fluid motion is so high as to make λ assume a very small value if compared with *L*. In this type of turbulence, we can isolate a vast subset of disturbances of much smaller scale length r of *L* (and consequently homogeneous, isotropic and almost stationary) but a lot greater than the Kolmogorov length λ. For these disturbances, the relative velocities v_r will be much greater than v_λ and therefore the relative Reynolds number $Re = v_r \, r \, / v$ will be very high with respect to $Re = v_\lambda \, \lambda \, / v = 1$. In other words, in this dimensional subinterval, the dominant process is the inertial transfer of energy to small-scale disturbances, without however any appreciable conversion of energy directly into heat by the viscous forces. The statistical properties corresponding to this sub-range of scale (known as Inertial Range) therefore do not depend on the viscosity v.

This is Kolmogorov's Second Hypothesis:

In the case of turbulence with a sufficiently high Reynolds Re number, the multidimensional probability distribution for the velocities in a sufficiently small space and in intervals $r \ll L$ and $\tau_k \ll L/U$ are determined, unambiguously, only by the value of the turbulent energy dissipation rate ε and are independent of the viscosity v.

This description implies a cascade transfer through an energy flow that defines the average rate of kinetic energy dissipated (ε) from the largest scales of motion towards smaller and smaller ones up to the dissipative scales where viscosity transforms all energy into heat. This interval is called inertial because it does not depend on either forcing or dissipation (v).
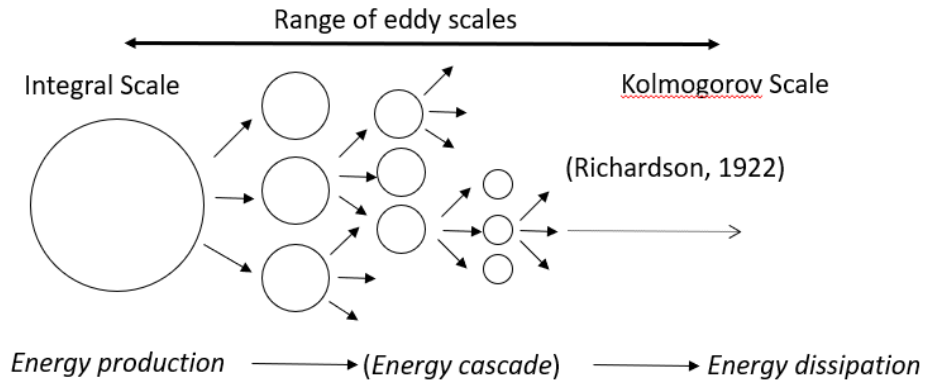
Fig. 9 – Kolmogorov hypothesis of the cascade of energy

Where $T_L = L/U$ is the time scale of large scale of flow.

Considering at this point an L_D scale length ($L_D = 60\,\lambda$) it is possible to divide the entire dimensional range in this way:

- Universal Equilibrium Range: $r < L_E$
- Inertial Range: $L_E > r > L_D$
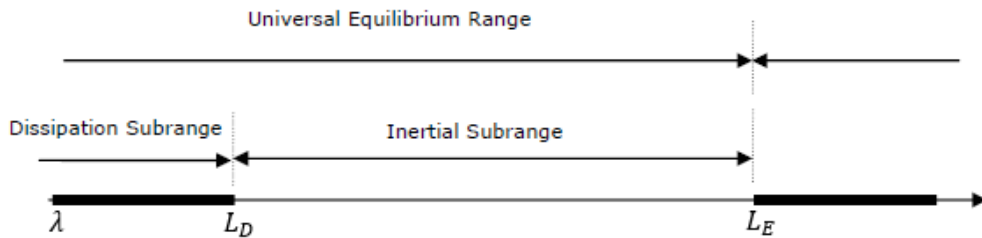- Dissipation Range: $r < L_E$

Fig. 10 – Division of dimensional range of turbulent disturbances

These relationships allow us to estimate the relationships between the characteristics of the largest and smallest scales in a turbulent flow as a function of the Reynolds number only.

The dynamics of intermediate structures with dimension r such that $L \gg r \gg \lambda$ (or in time using "s" such as $T_L \gg s \gg \tau_\lambda$), was considered by Kolmogorov's third hypothesis inspired by the observation that the dynamics of turbulence depends on how quickly energy is transferred from large to small scales and from the value of the viscosity that.

Introducing the wave number k where the cut is made in the transfer of power, and considering that for sufficiently high Reynolds numbers the characteristics (the statistics) of the structures of dimension r (with $L \gg r \gg \lambda$) are universal and depend solely on ε (and therefore are independent of ν), we can derive the famous power law ($k^{-5/3}$) for the energy spectrum:

$$K = \int_0^\infty E(k)dk \qquad (1.30)$$

where K is the kinetic energy per mass unit of the flow, from Kolmogorov's third hypothesis and from dimensional arguments we obtain:

$$E(k) = \mathcal{C} \; \varepsilon^{2/3} k^{-5/3} \qquad (1.31)$$

where $\mathcal{C}$ is a universal constant.

Particularly, the power dissipated in the homogeneous and isotropic turbulence follows a power law of the type:

$$P \approx f^{5/3} \qquad (1.32)$$
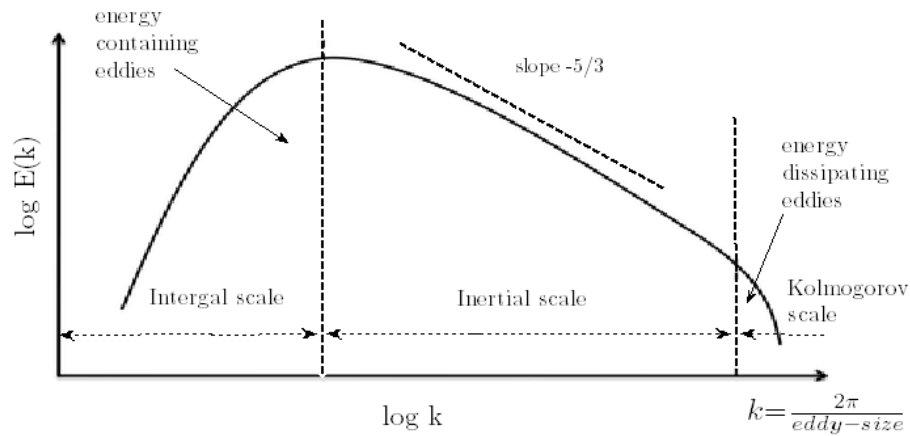
Fig. 11 – Kolmogorov hypothesis to the energy transferred from a bigger scale to a smaller one.

32

Chapter II – Motivation & Objectives

In the chemical industry, most of the processes involve mixtures of solid and fluid.

In these circumstances, the behaviour of solid particles in a turbulent fluid is not properly defined and further improvement would be necessary to the equipment design.

Several fundamental studies were carried out on the effects of the continuous phase acting on dispersed particles, but inconclusive results were reported, probably due to the limited experiment range of physical and operating conditions examined [13].

The multiphase flows involving a suspension of particles in the liquid were carried out under turbulent conditions of varying intensity in processing vessels, such as loop reactors and mechanically agitated vessels. Often in these processes, uniform dispersion of particles is achieved due to the interaction between turbulent eddies and the disperse phases. A better understanding of such interaction is fundamental to the effective design, modelling and operation of multiphase systems [6].

The difficulty in the modelling of the sedimentation, suspension and fluidisation phenomenon is related to the complexity of the structure formed by free-stream turbulence, which does not allow to predict the exact particles' motion.

From a mathematical point of view, the detailed description of the transition from laminar to turbulent flow is a complex problem; as the Reynolds number increases, a laminar flow becomes unstable, consequently the possibility that small perturbations evolve in a chaotic manner giving rise to the turbulent motion.

A fluid exerts a drag force on the particle that can be calculated by Stokes' law, in cases of a regime of motion with low values of Reynolds. When Reynolds increases, Stokes' law is no longer valid, and consequently, the relationship between drag coefficient (C_D) and number of Reynolds is not linear.

Due to the underlying non-linear nature of turbulent flows and the fact that a larger number of particles are present, an analytical solution to the problem cannot be expected. A possible way to investigate the problem, in case of industrial interest, is to considerer a statistical

description of turbulent motion, based on the solution of a mediated equation using a Stochastic Differential Equation (SDE).

Langevin in 1908 proposed a Stochastic Differential Equation (SDE) to describe the homogeneous and isotropic turbulent flows. This has been used, in this works, to describe the fluid' motion (§ 3.2).

The aim of this work is to define a correlation to describe the phenomenon of the particles settling, able to provide settling velocity data to compare with experimental data obtained from simulations.

The proposed correlation includes parameters that coming out from the previous studies mentioned above (§ 1.2).

$$\frac{U_s}{Ut} = f\left(\frac{d_p}{\sigma\, T_L}, \frac{\sigma}{U_t}, \frac{\Delta\rho}{\rho_f}, \frac{t_r}{T_L}, \frac{g\,\Delta\rho\, L}{\rho_f\,\sigma}\right) \qquad\qquad (2.1)$$

The final correlation will be better described in Chapter 4.

Chapter III – Methodology

3.1 Introduction

Langevin dynamics has been used in this work to describe the random motion of the turbulent flow. This model is constituted by Stochastic Differential Equations (SDEs) that are differential equation in which one, or more, terms include a random variable. These terms represent stochastic processes or the probabilistic version of a dynamic system, allowing to quantify parameters varying in a causal manner over time.

By carrying out multiple tests, the most probable value of a random variable is identified by considering its mean with a gaussian trend, which is characterized with a relative index of deviation or standard deviation from the expected value.

In this work, homogeneous and isotropic turbulence with zero mean flow has been considered.

The turbulent motion in these conditions can only occur in the absence of physical boundary limits or externally imposed mean flows; the structure of the velocity field, in terms of statistical quantities, is invariant under translation (homogeneity) and rotation (isotropy) of the reference system, with respect to which the motion of the fluid is being described. Only in these conditions, the chaotic motion of the fluid can develop freely, according to the dynamics imposed by the equations of motion.

The conditions of homogeneous and isotropic turbulence are ideal, thus rarely occur in practical applications. It can be assumed that the structure formed in chaotic motion at sufficiently small scales, existing at high Reynolds number, in small regions of space and for short duration intervals, is practically homogeneous and isotropic.

Fluid's motion can be described decomposing its instantaneous velocity in two terms, an average value and a fluctuation one.

By imposing stationarity for velocity's average value, the signal can be expressed as:

$$u(x,t) = U(x) + u'(x,t) \qquad (3.1)$$

$U(x)$ is the average value, while signal no-stationarity is given by fluctuation term $u'(x,t)$. Fig. 12 shows the decomposition of the signal in part medium and fluctuation.
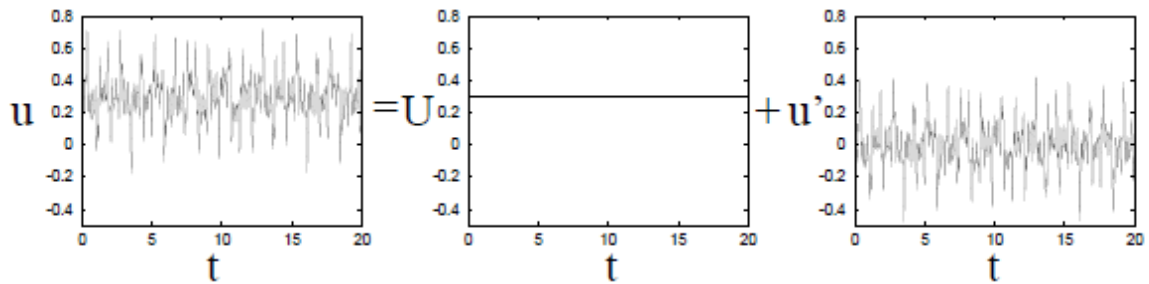
Fig. 12 – Reynolds decomposition of a statistically stationary signal in part medium and part floating [12].
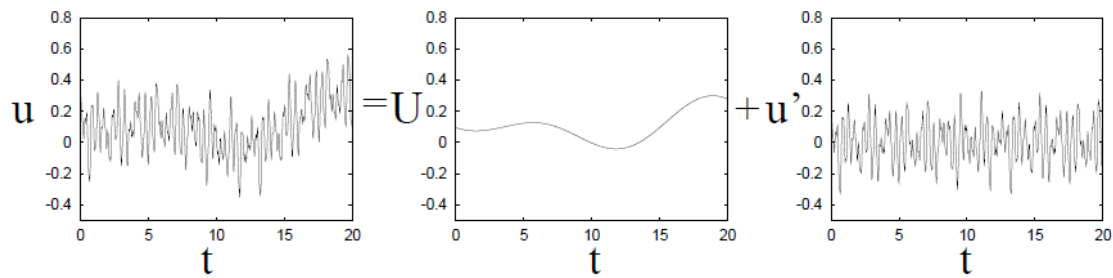
Fig. 13 – Decomposition of a statistically non-stationary signal in part medium and part floating [12].

If the average velocity is also a function of time, then the average operation should not be carried out for an infinite time, but over a finite interval which is very large compared to the time scales of the fluctuations, but rather short if compared with the times of variation of the mean-field (Fig. 13).

3.2 Langevin Equation

In the case of homogeneous, isotropic and statistically stationary turbulence by artificial force, the values of κ (kinetic energy) and ε (average rate of dissipated kinetic energy) are constant, with zero mean velocity. These premises allow to consider the particles of fluids all with the same characteristics, and it is, therefore, sufficient to consider a component of the velocity of the fluid particle $U^+(t)$, seen as the composing of velocity with a Lagrangian point of view.

The Langevin equation considers the velocity of microscopic-sized fluid particles following a Brownian-like motion. The stochastic processes $U^*(t)$ obtained from the Langevin' equation are called Ornstein-Unlenbeck (UO) processes, characterizing a Probability Density Function (PDF) [15].

Considering Eq.(3.2.1), the deviation u' presents an irregular, unpredictable trend and can be considered a random variable. It is possible to associate a difference density function $p(u')$ to the gap such that the product $p(u')du$ represents the probability that the random variable u' assumes the value between u' and $u' + du'$.

The probability P that the random variable assumes a value within a finite range $-u'_0 \leq u' \leq u'_0$ will, therefore, be given by:

$$P(u') = \int_{-U'_0}^{U'_0} p(u')du' \tag{3.2.1}$$

Referring to Fig.14, which shows a time course of a velocity difference, the interval of the values assumed by the difference must be divided into equal parts with an amplitude equal to $\Delta u'$. Subsequently, considering an interval of values of u' prime between $(k-1)\Delta u'$ e $k\Delta u'$, it must quantify the interval of time during which the random variable assumes values included in that interval. Said τ_k this interval and T_L the duration of the experiment or better the time interval for which the stochastic process $X(t)$ loses correlation with the value possessed at the initial instant, the ratio τ_k/T_L provides an approximate estimate of the probability that the variable u' prime takes values between $(k-1)\Delta u'$ e $k\Delta u'$.
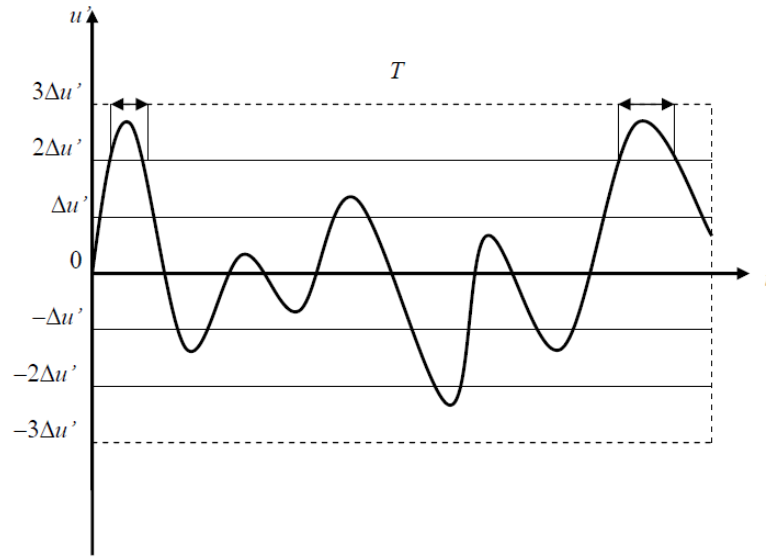
Fig. 14 – Deviation of velocity during the time [9].

Consequently, the sum of all τ_k is equal to the total duration of the experiment. This condition can be expressed by referring to the probability density estimate:

$$\sum_k \left(\frac{\tau_k}{T_L \, \Delta u'} \right) \Delta u' = 1 \qquad (3.2.2)$$

Knowing the probability density function (PDF) associated with the event in question, we can define the expected or average value of the random variable:

$$\langle u' \rangle = \int_{-\infty}^{\infty} u' \, p(u') \, du' \qquad (3.2.3)$$

The expected value of the velocity difference is zero, in fact, by approximating the letter integral with a summation we have:

$$\sum_k u_k' \left(\frac{\tau_k}{T_L \, \Delta u'} \right) \Delta u' = \frac{1}{T_L} \sum_k u_k' \, \tau_k \qquad (3.2.4)$$

Where u_k' prime is the average value assumed by the velocity difference in the time interval τ_k. The sum is made up of positive and negative products, which when added together give zero results.

The expected value of the velocity u obviously coincides with the average value U, introduced above.

38

$$\sigma^2 = \int_{-\infty}^{\infty} u'^2 \, p(u')du' \qquad (3.2.5)$$

The mean square deviation is defined as the quantity being diffusion processes not differentiable, the standard tools of differential calculus cannot be applied. Instead of differential calculus, the appropriate method is the Ito calculus; and, instead of being described by ordinary differential equations, diffusion processes are described by stochastic differential equations.

The infinitesimal increment of the process $U(t)$ is defined by:

$$dU(t) \; = \; U(t + dt) - U(t) \qquad (3.2.6)$$

where dt is a positive infinitesimal time interval.

For the Wiener process, in particular, it possible to consider:

$$d\,W(t) \; = \; W(t + dt) - W(t) \stackrel{D}{=} \mathcal{N}(0, dt) \qquad (3.2.7)$$

The symbol $\stackrel{D}{=}$ is read as "is equal in distribution to", and $\mathcal{N}(\mu, \sigma^2)$ is the normal distribution, in particular, denotes the normal with mean μ and variance σ^2.

Now consider the process $U(t)$ defined by the initial condition $U(t_o) = U_o$ and by the increment:

$$dU(t) \; = \; a[U(t), t] \, dt \; + \; b[U(t), t] \, dW(t) \qquad (3.2.8)$$

For given functions $a(V, t)$ and $b(V, t)$. It is readily verified that the process $U(t)$ defined by this stochastic differential equation is a diffusion process, and, as implied by the notation, the drift and diffusion coefficients are $a(V, t)$ and $b(V, t)$ [15].

A random variable is fully characterized by its probability density function (PDF), and two random variables with the same probability density function (PDF), are statistically identical. Similarly, a diffusion process is fully characterized by its drift and diffusion coefficients; and two diffusion processes with the same coefficients are statistically identical [15].

Thus, the stochastic differential equation Eq. (3.2.9) provides a general expression for a diffusion process. It shows that the infinitesimal increment of a diffusion process is Gaussian, i.e.,

$$dU(t) = \mathcal{N}(a[U(t), t]dt, b[U(t), t]^2 \, dt) \tag{3.2.9}$$

This Gaussian is not a defining property of diffusion processes, but rather a deduction from their definition [15].

The Langevin equation denotes this velocity mentioned above as $U^*(t)$, thus obtaining:

$$dU^*(t) = -U^*(t)\frac{dt}{T_L} + \left(\frac{2\sigma^2}{T_L}\right)^{\frac{1}{2}} dW(t) \tag{3.2.10}$$

where T_L is the Lagrangian integral time-scale e σ^2 is the variance, both constant.

The Eq. 3.2.10 can be express through the finite-difference equation:

$$U^*(t + \Delta t) = U^*(t) - U^*(t)\frac{\Delta t}{T_L} + \left(\frac{2\sigma^2 \, \Delta t}{T_L}\right)^{\frac{1}{2}} \xi(t) \tag{3.2.11}$$

Where the first term is related to the dissipation coefficient which causes the velocity to relax towards zero on the timescale T_L, while the second term is called random coefficient and it is the statistical refers to a random increment to zero-mean of the standard deviation σ^2. The term $\xi(t)$ is the standardized Gaussian random variable, which is independent of itself at different times and which is independent of $U^*(t)$ at the last time.

The constant diffusion coefficient:

$$a(U^*, t) = -\frac{U^*}{T_L} \tag{3.2.12}$$

Considering the random coefficient $dW(t) = 0$, and integrating the Langevin equation:

$$\int_0^t dU^* = -\int_0^t \frac{U^*}{T_L} dt \tag{3.2.13}$$

$$ln\frac{U_t^*}{U_0^*} = -\frac{t}{T_L} \rightarrow U_t^* = U_0^* \, exp\,(-t/T_L) \tag{3.2.14}$$

Which means that the velocity would be totally dissipated during the time (back curve in Fig. 15).

The constant diffusion coefficient:

$$b(U^*, t) = \left(\frac{2\sigma^2}{T_L}\right)^{\frac{1}{2}} \tag{3.2.15}$$

The random coefficient implies that fluid has a random motion, with normal distribution σ^2.
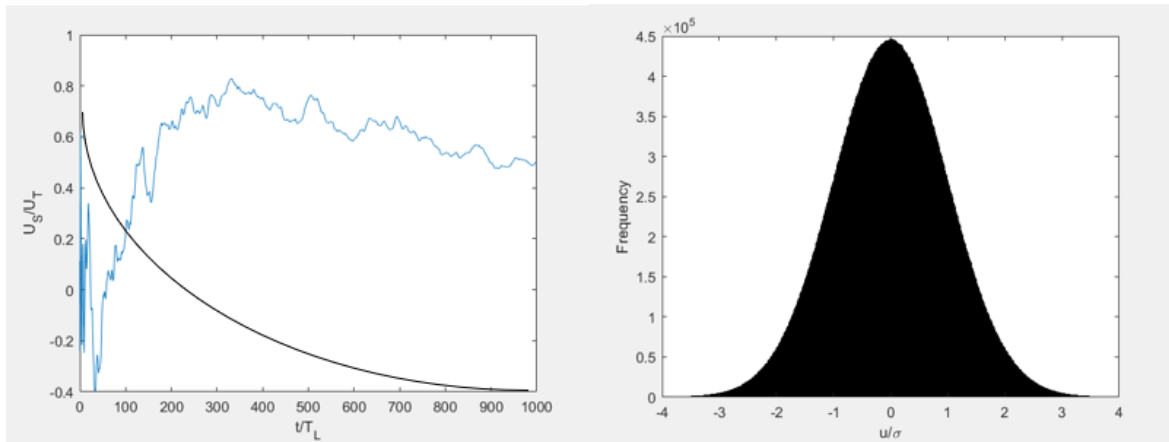
Fig. 15 – The right plot is the velocity of the fluid obtained by the Langevin equation, where the purple curve is due to the dissipation term and the blue curve is due to the random term. At left the Gaussian curve of distribution velocity.

Plotting the Langevin equation is possible to evaluate that U^* is a statistically stationary and a Gaussian process, that is characterized with an average at zero, with variance σ^2 and, in particular with an autocorrelation function given by:

$$\rho(s) = e^{-|s|/T_L} \tag{3.2.16}$$

The autocorrelation function is the correlation of a signal with a delayed copy of itself as a function of delay. Informally, it is the similarity between observations as a function of the time lag between them.

If this is the autocorrelation function of the Lagrangian velocity, its Lagrangian integral timescale is defined by:

$$T_L = \int_0^\infty \rho(s)\,ds \qquad (3.2.17)$$

If the equation relatives at autocorrelation function are consistent with this definition the T_L the coefficient in the Langevin equation is indeed the integral timescale of the process.

The Langevin equation is correct in yielding a Gaussian probability density function (PDF) of velocity. In isotropic turbulence, the one-time PDF of the Lagrangian velocity $U^+(t)$ is identical to one-point, one-time Eulerian PDF as demonstrated from experiment and DNS (direct numeric simulation), where PDF's are very close to Gaussian [15].

The correct variance is defined by:

$$\sigma^2 = \frac{2}{3}\kappa \qquad (3.2.18)$$

Considering high-Reynolds number of turbulence in which there is a large separation between the integral timescale T_L and the Kolmogorov time scale τ_η, it has been examined $U^+(t)$ on inertial-range timescales "s", $T_L \gg s \gg \tau_\lambda$. This is best done through the second-order Lagrangian Structure Function:

$$D_L(s) \equiv \langle\, [U^+(t+s) - U^+(t)]^2 \rangle \qquad (3.2.19)$$

With this function, which is just the variance of the increment over the time interval $s > 0$, it is possible to express the autocorrelation of the velocity of a particle, and, particularly, being Lagrangian, it follows the trajectory of a particle taken individually.

The second-order Lagrangian Structure Function D_L, for Kolmogorov's hypothesis, is proportional to "s" in the inertial range, and also at the rate of dissipation of the turbulent kinetic energy as follows:

$$D_L(s) = C_o\, \varepsilon\, s \quad \text{per} \quad T_L \gg s \gg \tau_\lambda \qquad (3.2.20)$$

Where C_o is the Kolmogorov constant, whereas the Langevin equation yields:

$$D_L(s) \equiv \langle\, [U^*(t+s) - U^*(t)]^2 \rangle \qquad (3.2.21)$$

$$= \frac{2\sigma^2}{T_L} s \quad \text{for} \quad s \ll T_L \tag{3.2.22}$$

Thus, the Langevin equation is consistent with the Kolmogorov hypothesis in yielding a linear dependence of D_L on "s" in the inertial range.

In place of σ^2 e T_L, in the Langevin equation, it is possible to use the terms kinetic energy (κ) and an average rate of dissipated kinetic energy (ε) and introducing the Langevin-model constant C_o through the relation:

$$\frac{2\sigma^2}{TL} = C_o\, \varepsilon \tag{3.2.23}$$

$$T_L^{-1} = \frac{C_o\, \varepsilon}{2\, \sigma^2} = \frac{3}{4}\, C_o\, \frac{\varepsilon}{\kappa} \tag{3.2.24}$$

Defined those constant, it has been used again to express the Langevin equation as:

$$dU^*(t) = -\frac{3}{4}\, C_o\, \frac{\varepsilon}{\kappa}\, U^*(t)\, dt + (C_o\, \varepsilon)^{\frac{1}{2}}\, dW(t) \tag{3.2.25}$$

It is straightforward to incorporate Reynolds-number dependence in the Langevin model simply by making the model coefficient C_o depend on Re_T, therefore, $C_o(Re_T)$. Consistency with the Kolmogorov hypotheses requires only:

$$\lim_{Re_T \to \infty} C_o(Re_T) = C_o \tag{3.2.26}$$

where now we distinguish between the Kolmogorov constant C_o and the model coefficient $C_o(Re_T)$. Furthermore, $C_o(Re_T)$ can be determined directly from DNS data by Eq.33, that can be reorganized as:

$$C_o = \frac{4\, \kappa}{3\, \varepsilon\, T_L} \tag{3.2.27}$$
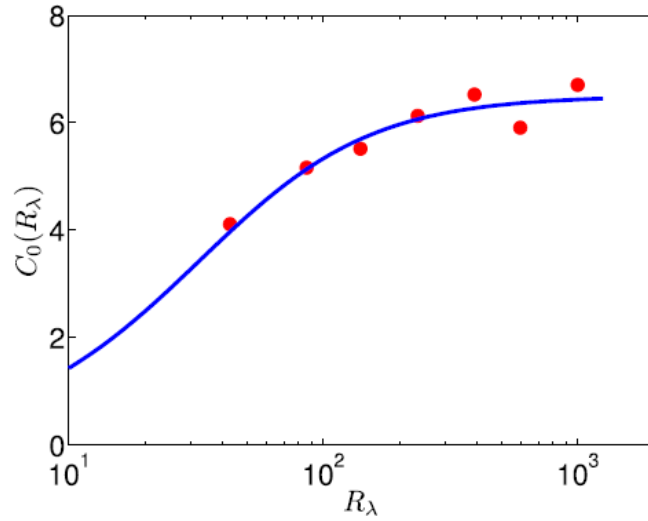
Fig. 16 – The Langevin-model constant C_o against Reynolds number. Symbols (●) from Eq.2*; Empirical fit (━) from Eq. 38.

The values of C_o were obtained from Direct Numerical Simulation (DNS), compared to the empirical fit, which is based on a suggestion by Sawford et al. [16].

$$C_o(Re_T) = \frac{6.5}{(1 + 140\ Re_T{}^{-4/3})^{3/4}}$$

(3.2.28)

From Fig. 16, the fit represents the data which is consistent with the Kolmogorov hypotheses with $C_o = 6{,}5$.

$$\sigma = \sqrt{\frac{2}{3}k}$$

(3.2.29)

$$Re_T = \sqrt{\frac{15\ \sigma}{\frac{\varepsilon\ \mu}{\rho}}}$$

(3.2.30)

Re_T is the Taylor-Scale Reynolds number which is sometimes called the turbulence length scale, is a length scale used to characterize a turbulent fluid flow. The Taylor microscale is the intermediate length scale at which fluid viscosity significantly affects the dynamics of turbulent eddies in the flow.

$$T_L{}^{-1} = \frac{3}{4}\ C_o\ \frac{\varepsilon}{\kappa}$$

(3.2.31)

$$t_r = \frac{\frac{\rho_p}{\rho_p + 0.5} d_p}{\frac{3}{4}\left(\frac{\rho_f \, d_p \, |U_t|}{\mu}\right)|U_t|} \tag{3.2.32}$$

t_r is the particle relaxation time, that is, the constant time in the exponential decay of the velocity of the particle due to the drag.

3.3 Kinematic of Settling

To describe the kinematic of the settling of particles with mass is necessary to consider all relevant forces acting on them. Furthermore, these particles will be equipped with motion with a trajectory that will surely depend on the motion of the fluid.

In order to describe particles' motion, a set of kinematic equations, involving forces balance, particle motion and Langevin equation were needed.

Langevin equation describes the fluid motion as stated in § 3.2.

$$dU^*(t) = -\frac{3}{4} \, C_o \, \frac{\varepsilon}{\kappa} \, U^*(t) \, dt + (C_o \, \varepsilon)^{\frac{1}{2}} \, dW(t) \qquad (3.2.25)$$

A solid particle immersed in a fluid undergoes to different forces acting on it, expressed by a balance equation:

$$\frac{dV}{dt} = \frac{3}{4} \frac{\rho_f}{\rho_s} \frac{C_D}{dp} (U - V)|U - V| + \frac{1}{2} \frac{\rho_f}{\rho_s} \left(\frac{dU}{dt} - \frac{dV}{dt}\right) + \left(\frac{\rho_s - \rho_f}{\rho_s}\right) g \qquad (3.3.1)$$

In the balance equation (3.3.1), forces acting on a single particle suspended in a turbulent fluid can be approximately evaluated from mean velocity fields of the fluid and the solid phases. Terms involved are drag force, virtual mass, and gravitational and buoyancy force, respectively.

U and V are fluid and particle velocity vectors, respectively, while ρ_s and ρ_f are particle and fluid densities. dp corresponds to the particle diameter, while g is the gravitational constant.

C_D is the drag coefficient, given by following equations.

$$C_D = \begin{cases} \dfrac{24}{Re} \, (1 + 0.15Re^{0.687}) & \text{for } Re \leq 1000 \\ 0.44 & \text{for } Re > 1000 \end{cases} \qquad (3.3.2)$$

$$Re = \frac{\rho_f \, dp \, |U - V|}{\mu_f} \qquad (3.3.3)$$

Eventually, particle velocity is described by the variation of its trajectory during the time.

$$\frac{dX_p}{dt} = V \tag{3.3.4}$$

These equations must be considered along with any cartesian coordinates (*x, y, z*).

3.3.1. Basset Force

In the balance equation, the terms relating to the Basset force has been neglected, following the observations proposed by Laurence Bergougnoux et al. (2014).

The work carried out by Laurence Bergougnoux et al. have presented a jointed experimental and numerical studies of the settling of small solid spheres in a cellular flow field at low Stokes number.

At low Stokes number ($St < 0.01$), using Stommel model, they were identified a Stokes regime for which the velocity of the particle was simply the sum of its Stokes velocity and the local fluid velocity given by the cellular flow.

At larger Stokes number (but still $St < 0.1$), the particle velocity is still described by the sum of the fluid velocity and the particle settling velocity. However, as the particle Reynolds number can be larger than unity, the drag is no longer the Stokes drag but becomes nonlinear and can be well reproduced by correlations such as that of Schiller-Naumann.

The particle trajectories ware analysed in terms of velocity ratio, especially, when this velocity ratio is much larger than unity, the particle trajectories were straight lines and the particles experience only small modulations coming from the vertical flow.

When this ratio is much smaller than unity, the particles are settling out but can become momentarily trapped in a cell. In between, the particle trajectories present more or less marked oscillations.

From the simple Stommel model with a Stokes drag and the full Boussinesq-Basset-Oseen model derived in the Stokes regime both overestimate the settling velocity.

In the regimes of Stokes number that they have explored, it was seen that Basset's force had a much smaller contribution than others, therefore, drag and buoyancy forces prevailed.

In this work, it has been decided to do not implement the Basset force in equation (3.3.1). It has been shown that this term has a limited impact on the kinematics of the particle, and it is not easy to implement numerally.

Chapter IV – Results

4.1 Simulations

Simulations, conducted on MATLAB™ programming software, aim to obtain reliable data about particle's settling velocity, to be compared to that deriving from correlation proposed. Several variables involved must be investigated in different assets, giving back accurate values of the term objective of this study.

In the context of defining fluid's motion, undergoing isotropic and homogeneous turbulence, Langevin stochastic differential equation has been involved.

As we have seen in § 3.2, Langevin equation is characterised as follows:

$$\overline{u(t)} = 0 \tag{4.1}$$

$$Var\big(u(t)\big) = \sigma^2 \tag{4.2}$$

The solution to this kind of equation is approximated by implementing in the programming software an iterative implicit method from literature. In this work, the Runge-Kutta's has been adopted.

$$dU^*(t) = a\,dt + b\,dW(t) \tag{4.3}$$

$$a = -\frac{U}{T_L} \tag{4.4}$$

$$b = \left(\frac{2\sigma^2}{T_L}\right)^{\frac{1}{2}} \tag{4.5}$$

It has been necessary to fix values for σ and T_L, namely variance and integral time scale, respectively. Tests conducted require boundary conditions, as the initial and final time of observation. Also, it is fundamental to determine the amplitude of time step of integration h that best fit values of the velocity signal.

T_L	σ	t_i	t_f	$h = \Delta t$
1	0.1	0	$G_t\, T_L$	$\dfrac{T_L}{N_t}$

Table 1 – Fixed parameters.

G_t is a multiplication factor that permits to test the phenomenon at different integral time scales, aiming to reach a reliable finale observation time, combined with a wide distribution of signal, useful to outline mean velocity trend.

N_t is a variable that splits observation time into many spans, catching the best value of mean velocity acting on them by choosing carefully its magnitude.

4.1.1 Tests set-up

Researches on parameters which affect fluid's velocity started from investigating velocity signal and probabilistic Gaussian distribution. The aim is to obtain a signal $\overline{u(t)}$ fluctuating around a single null value, giving back a distribution modelled on $\sigma = 0.1$. Also, the autocorrelation function must follow Eq. (3.2.16), and the power dissipated have to be in accordance with Kolmogorov's third hypothesis.

At first instance, in order to demonstrate fluid's isotropic and homogeneous turbulence introduced by Taylor, various tests have been conducted, by varying G_t and N_t. Assigning them random values, it is shown how signal and Gaussian trend are significantly affected.

$$\begin{cases} G_t = 1000 \\ N_t = 10 \end{cases}$$
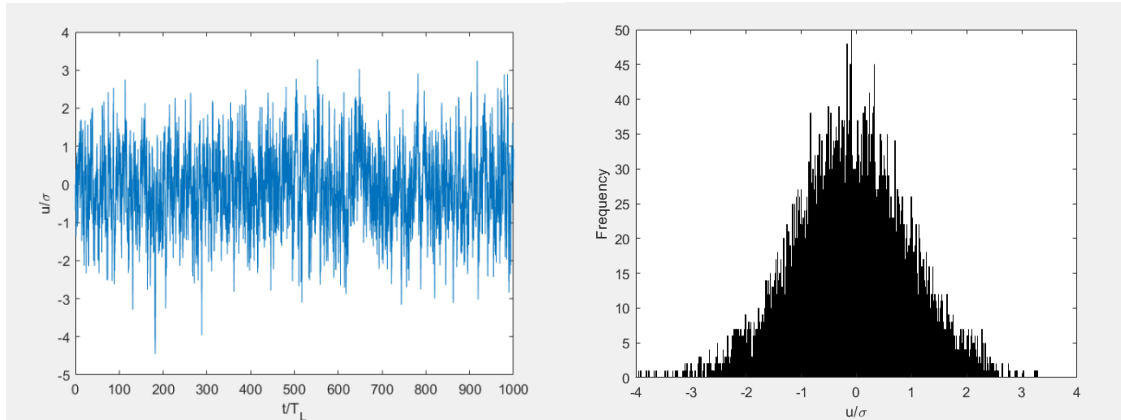
Fig. 17 – Plot mean velocity and standard deviation considering 1) condition

Fig.17 depicts how plots' shapes are not well-defined. In fact, applying the Langevin equation results obtained shows a slight deviation from the desired value.

$$\begin{cases} \overline{u(t)} = -0.010438 \\ \sigma = 0,099197 \end{cases}$$

In the optical of improving results, the value of G_t has been increased, keeping constant N_t.

$$\begin{cases} G_t = 1000000 \\ N_t = 10 \end{cases}$$
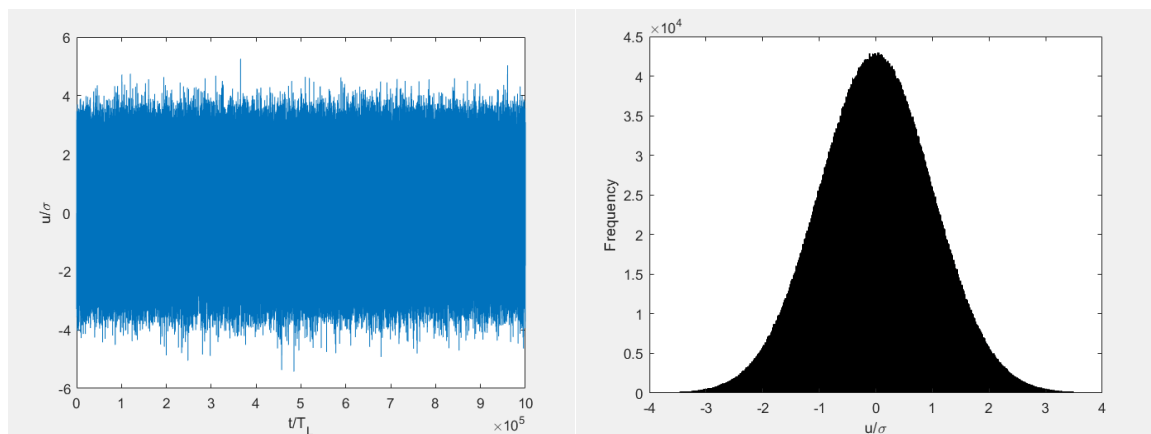
Fig. 18 – Plot mean velocity and standard deviation considering 2) condition

51

In this case, it can be seen how resulting plots are more defined, with mean velocity and variance closely to fixed values.

$$\begin{cases} \overline{u(t)} = 0.00016194 \\ \quad \sigma = 0.099985 \end{cases}$$

One can also choose to increase N_t, by imposing the same value for G_t, as done for the previous case.

$$\begin{cases} G_t = 1000000 \\ \quad N_t = 100 \end{cases}$$
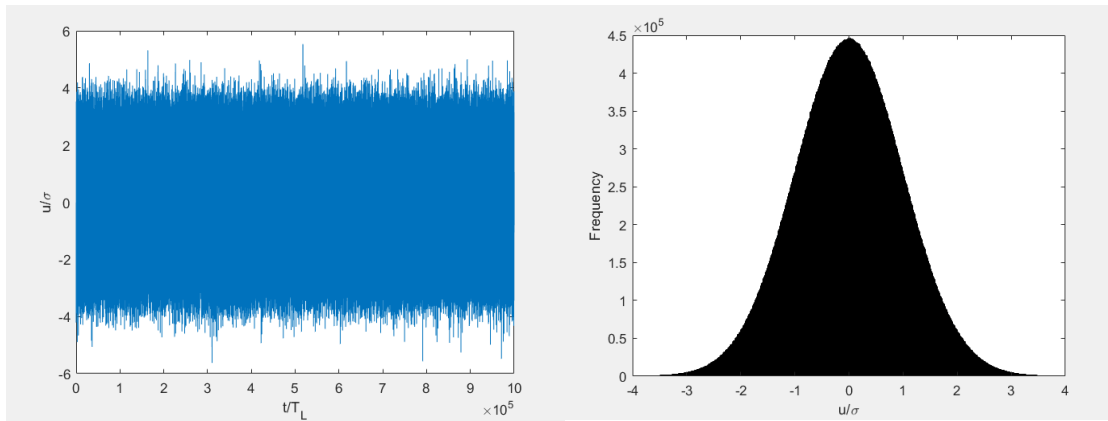
Fig. 19 – Plot mean velocity and standard deviation considering 3) condition

Plots are now clearly defined, suggesting that an increase of these values leads to the best statistical description of fluid's motion.

$$\begin{cases} \overline{u(t)} = -0.00015476 \\ \quad \sigma = 0.099992 \end{cases}$$

Results obtained imply that the last values adopted for the variables G_t and N_t provide $\overline{u(t)} \cong 0$ and $\sigma \cong 0.1$, with shapes of the plots (Fig.19) showing a narrowband signal and a more definite Gaussian trend.

A second instance, according to the definition of the autocorrelation function, that is the correlation of a signal with a delayed copy of itself as a function of delay, the condition imposed by Eq. (3.2.16) has to be fulfilled.

The trend of the autocorrelation function of velocity $u(t)$ against the dimensionless time (t/T_L) is plotted in (Fig. 20).
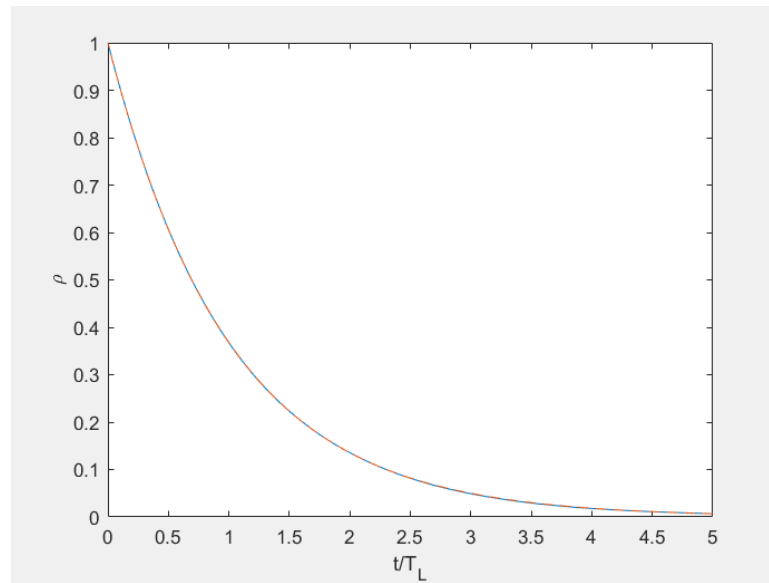
Fig. 20 – Autocorrelation function ρ, obtained from Direct Numerical Simulation (DNS), compared to the Eq.20.

It can be seen how the autocorrelation function curve of $u(t)$ (dotted red curve) follows perfectly the trend given by Eq. (3.2.16) for ρ (blue curve): in fact, they are exactly overlapping.

Eventually, according to Kolmogorov's third hypothesis, briefly described in § 1.4, the power dissipated' trend in the homogeneous and isotropic turbulence, expressed by Eq. (1.32), has been investigated.
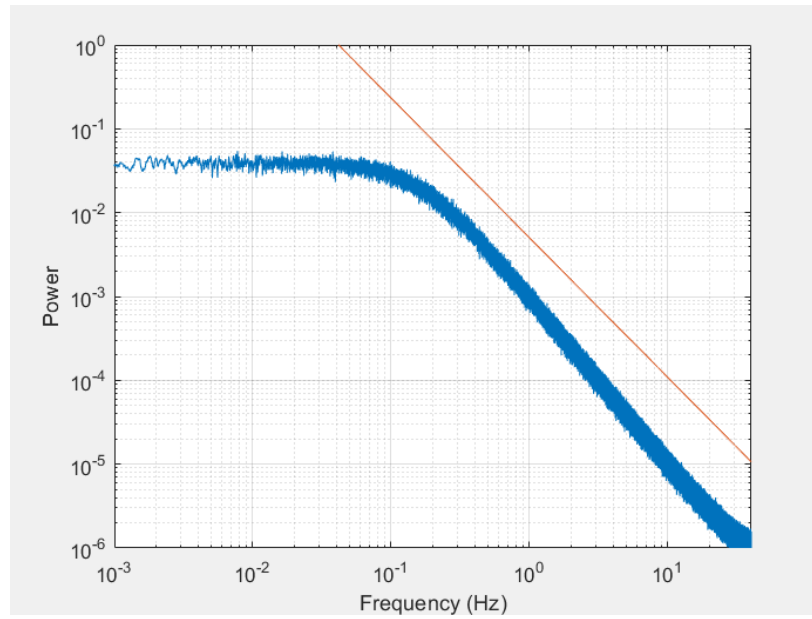
Fig. 21 – Plot of Power dissipated according to Kolmogorov third Hypothesis.

Fig. 21 shows the signal of power dissipated against Frequency (blue trend). For values of Frequency over 10^{-1} Hz, the signal follows the same trend of a function $f^{-5/3}$, given by Kolmogorov's hypothesis and depicted by a red line, reported for comparison.

Analysing results deriving from tests reported above, it is possible to conclude that fluid's turbulence behaviour is isotropic and homogeneous.

4.1.2 Particle without mass immersed in a homogeneous and isotropic turbulent flow

Once fluid's behaviour has been explored, analysis proceeds by considering adding in it a particle without mass.

It is fundamental to inquire how this particle interacts with fluid.

As done for the fluid in simulations reported § 4.1.1, a particle must follow the condition of isotropic and homogeneous turbulence.

Its motion over time and space has traced, by fixing the following boundary conditions:

$$\begin{cases} x(t) \\ y(t) \\ z(t) \end{cases} \qquad \begin{cases} \dfrac{dX}{dt} = u(t) \\ x(t=0) = (0,0,0) \end{cases} \qquad (4.6)$$

X(t) considers all the contributes dictated from the three dimensions.

At first instance, it has been studied if the particles follow the autocorrelation function, given by Eq. (3.2.16).

By setting:

T_L	σ	t_i	t_f	$h = \Delta t$
1	0.1	0	$G_t\, T_L$	$\dfrac{T_L}{N_t}$

Table 2 – Fixed parameters.

with $G_t = 1000$, and $N_t = 100$.

The autocorrelation function of $u(t)$ has been studied for each cartesian direction, as shown in Fig. 22 and according to the condition imposed by Eq. (4.6).
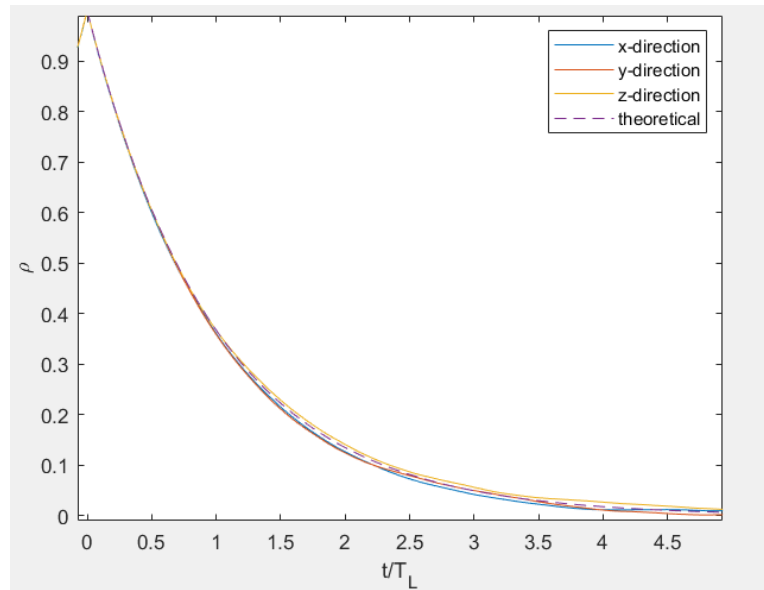
Fig. 22 – The three functions of autocorrelation function ρ, obtained from Direct Numerical Simulation (DNS), compared to the Eq.20.

Curves obtained in Fig. 22 (blue *x*-direction, red *y*-direction and yellow *z*-direction line) do not overlap, but they are close to the theoretical one given by Eq. (3.2.16) (dotted curve).

Results deriving from the simulation are here reported.

$$\begin{cases} \sigma(x) = 0.10369 \\ \sigma(y) = 0.10203 \\ \sigma(z) = 0.09514 \end{cases}$$

Values of variance are close to the fixed one of $\sigma = 0.1$.

The statistical realisation of trajectory in turbulent flow has been traced in Fig. 23. Considering the statistical approach, another realisation would have a completely different trajectory, due to the randomness of the model.
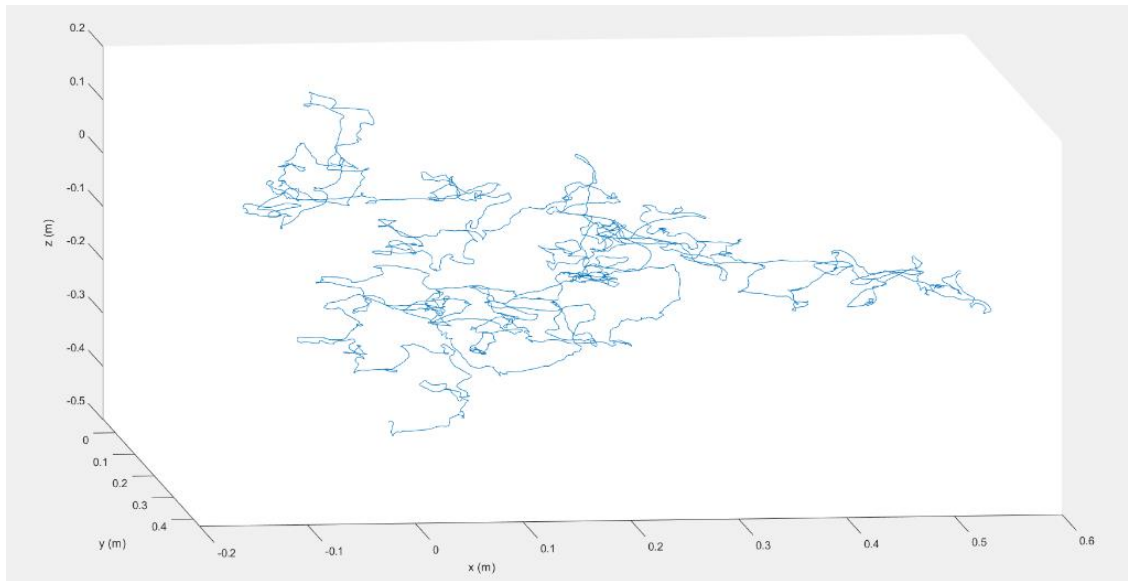
Fig. 23 – Plot of the motion of particle without mass immersed in a turbulent fluid.

The particles' motion is irregular, due to its random motion, as clearly shown by Fig. 23.

4.1.3 Particle with mass immersed in a homogeneous and isotropic turbulent flow

The fluid dynamics of the system has been analysed by looking at the physical affection between fluid and solid particle. For this reason, in this section, the cases of a study presented consider adding a particle with mass, in the same fluid analysed in the previous paragraphs.

Starting from the knowledge that a particle-with-mass velocity in the turbulent fluid could be different from that in the still fluid, it is essential to characterise its trend over time.

In the end, the statistical motion of the particle and its position along time has been plotted.

Aiming to reach the best statistical description of the phenomenon, two cases of study have been explored, differing from each other by particle's number involved.

Langevin equation, crucial to describe fluid's field of motion, and force balance, written to explain what forces act on the particle (§ 3.3), are essential for these cases of study.

Following conditions are shared for both cases.

T_L	σ	t_i	t_f	$h = \Delta t$
1	0.1	0	$G_t \, T_L$	$\dfrac{T_L}{N_t}$

Table 3 – Shared conditions for both cases of study.

4.1.4 Cases of study

First Case

Subsequent parameters have been set-up:

n_p	k	ε	μ	d_p	ρ_p	ρ_f
1	0.1	10	1×10^{-3}	$0.5 \cdot 10^{-3}$	2000	1000

Table 4 –Parameters set-up.

All parameters are considered in S.I units.

with different conditions imposed:

1) $\begin{cases} G_t = max(1000 \cdot T_L, 5 \cdot t_r) \\ N_t = T_L/100 \end{cases}$

2) $\begin{cases} G_t = max(1000 \cdot T_L, 5 \cdot t_r) \\ N_t = T_L/50 \end{cases}$

Particle's-with-mass velocity trend overt time, for the condition mentioned above, is reported in Fig. 24.
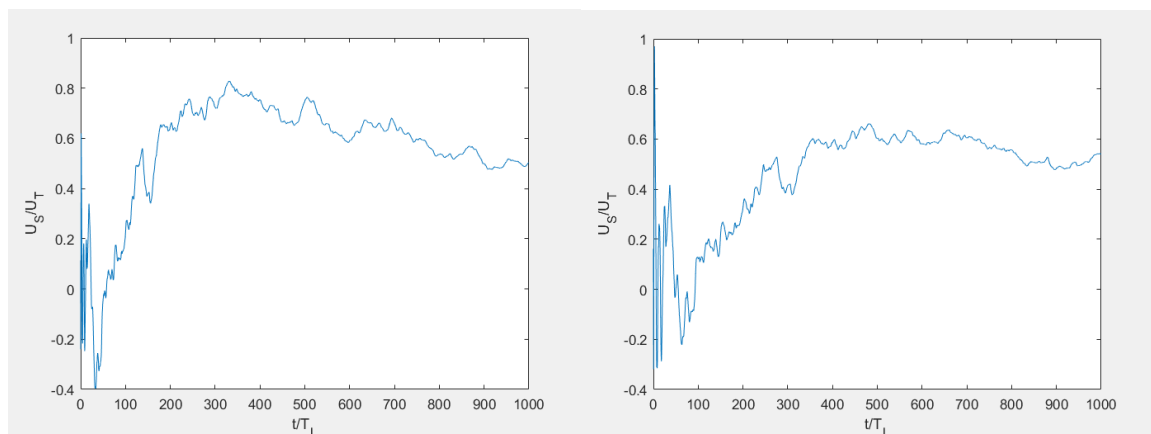
Fig. 24 – Plot of the ratio of settling velocity and that in still fluid against the ratio of t/T_L. Plot on the left refers to the first asset, while that one on the right refers to the second one.

In Fig. 24, the ratio between settling velocity in turbulent fluid and that in the still fluid presents uncertainty, dictated by the strong fluctuations that signal shows over time. This may limit future simulations; hence it leads to unclearly evaluations of velocity.

Particle's statistical settling among z-axis presents discrepancies, with respect to the two conditions.
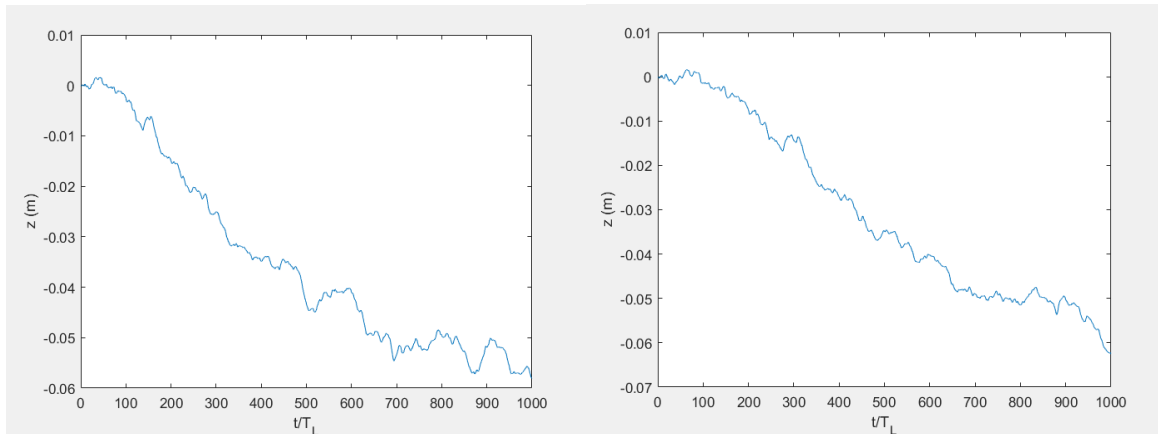
Fig. 25 – Plot of the statistical altitude change over time. The plot on the left is obtained by considering the first condition, instead, the plot on the right is considering the second one.

From Fig. 25, it is possible to realize that the particle's motion is uncertain. In fact, curves do not follow a comparable path, thus conceiving a statistical realistic settling through simulating only one particle is not credible.

The typical particle's statistical motion among three-dimensions is illustrated in Fig. 26.
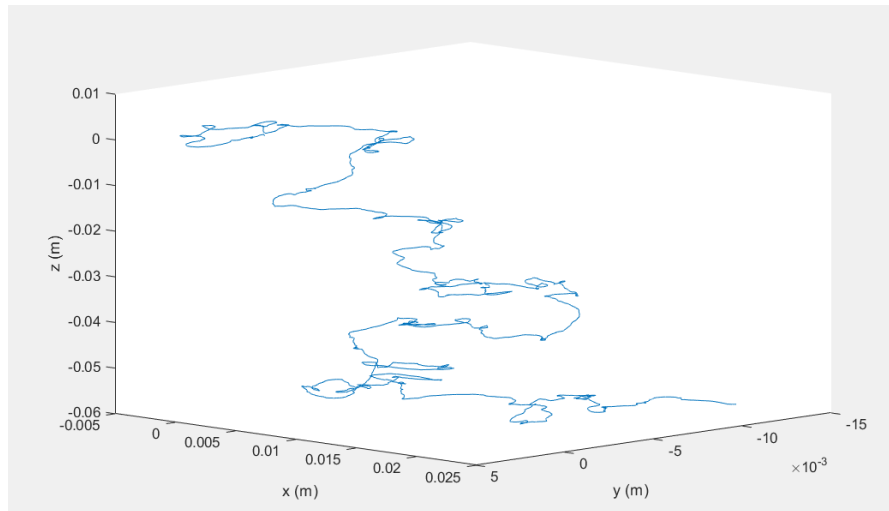
Fig. 26 – Plot of the statistical movement of the particle.

Second Case

The second case of study involves 1000 particles, with the same characteristics stated for the first one.

Subsequent parameters have been set-up:

n_p	k	ε	μ	d_p	ρ_p	ρ_f
1000	0.1	10	1×10^{-3}	0.5×10^{-3}	2000	1000

Table 5 –Parameters set-up.

All parameters are considered in S.I units.

with following conditions considered.

$$\begin{cases} G_t = max(1000 \cdot T_L, 5 \cdot t_r) \\ \quad N_t = T_L/100 \end{cases}$$

61

The ratio between the particle's settling velocity in turbulent fluid and that in the still one has been plotted over time (Fig. 27).
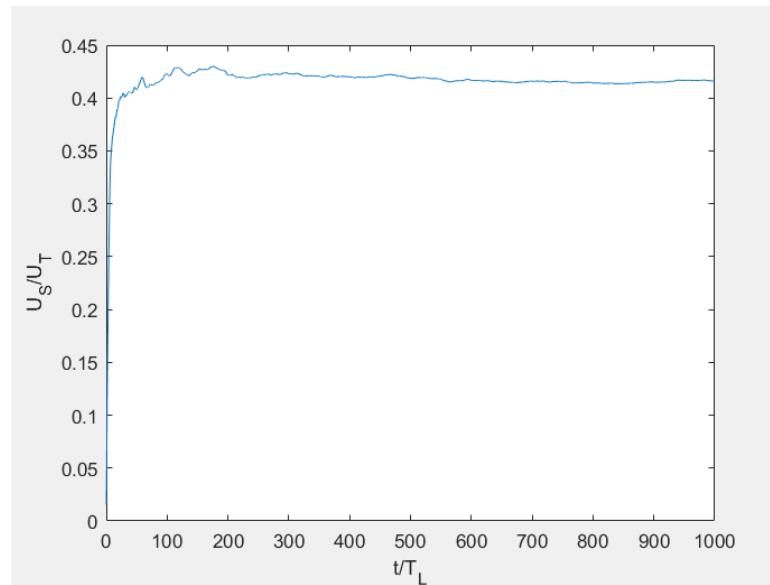
Fig. 27 – Plot of the ratio of settling velocity and that in still fluid obtained by simulation against the ratio of t/T_L.

The trend of the ratio shows an asymptotic value of the signal; it means that one can extrapolate a constant statistical value, after an initial time.

The statistical motion of 1000 particles among the z-axis is reported versus time in Fig. 28.
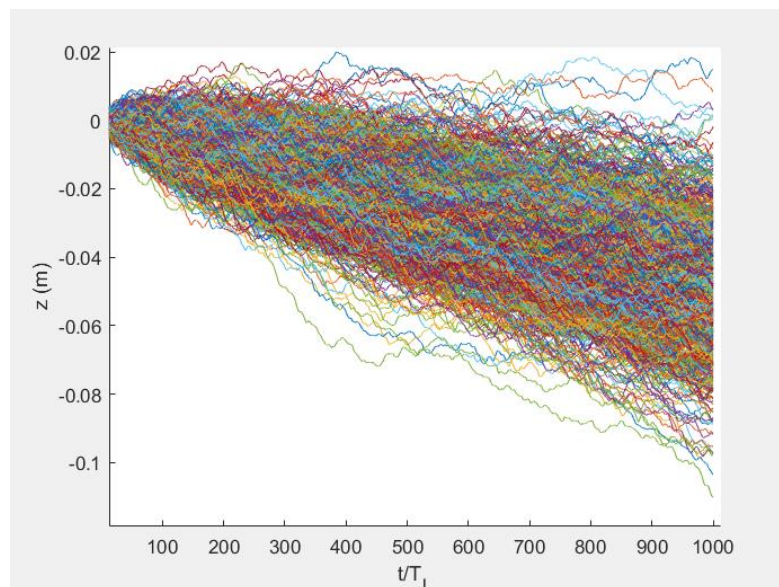
Fig. 28 – Plot of the statistical altitude change over time.

Fig. 29 shows the average and the curves for $+/-$ two times the standard deviation values of the previous plot.
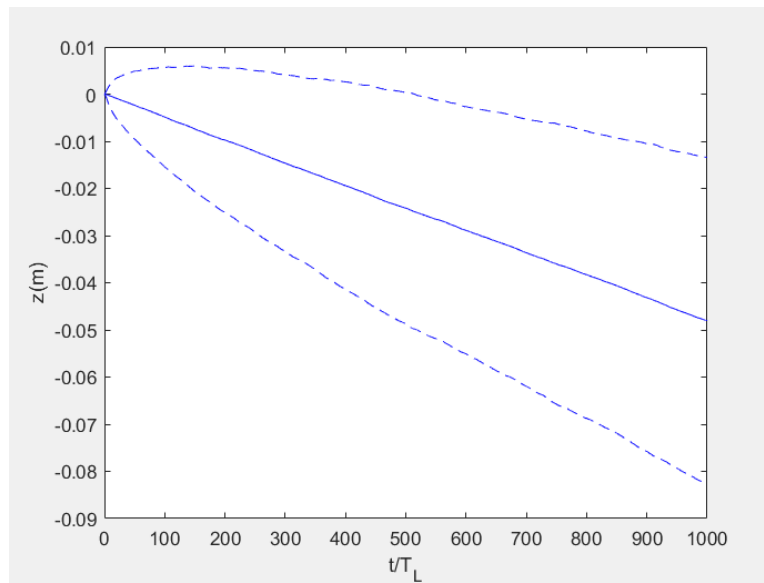
Fig. 29 – Plot of the statistical altitude change over time. Continuous line indicates the mean movement of the total particles.

Velocity's standard deviation of particles has been compared with the standard deviation σ_u, characteristic of an isotropic behaviour, for each direction in physical space.
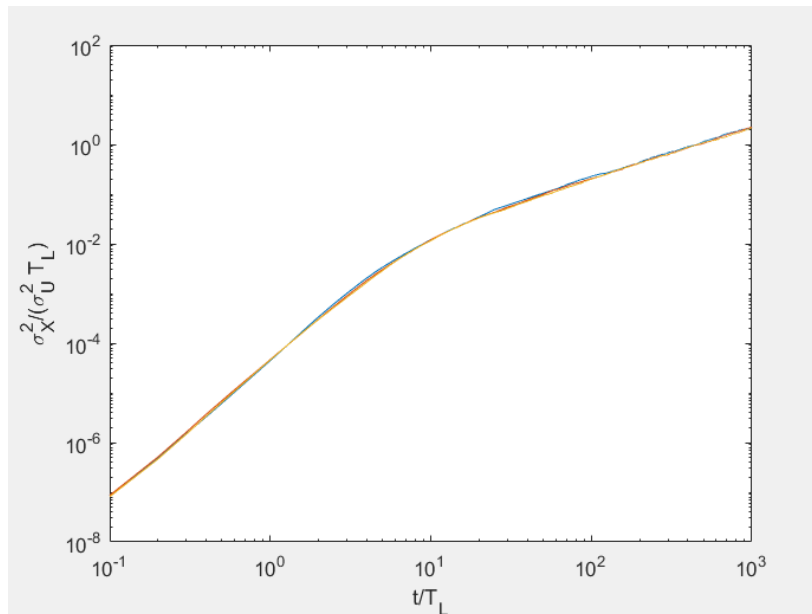
Fig. 30 –Standard deviation of velocity for each direction in physical space against t/T_L.

It can be seen how curves of velocity's standard deviation are close to that one characteristic of isotropic behaviour. Over the value of $10\ T_L$, the standard deviation of velocity reaches steadily conditions, with zero mean velocity of the particles $\langle Us \rangle = 0$.

Particle's deviation from their mass centre at different altitudes (Z) has been illustrated (Fig. 31).
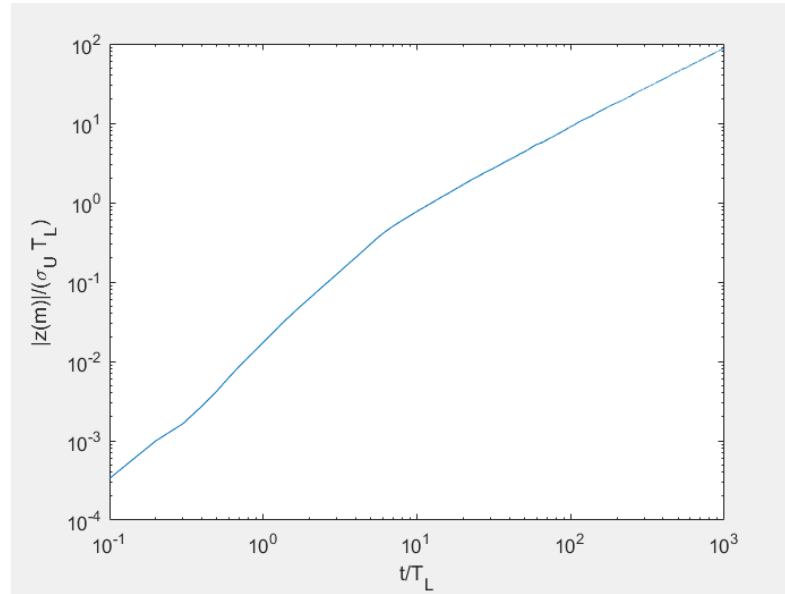
Fig. 31 – Mean movement of particles in altitude against t/T_L.

It is clear from Fig. 31 how particles require times greater than $10\ T_L$ to get a steady value of apparent terminal velocity.

Initially, when the particle's movement starts, they are very close to each other; after a certain time, they move to another point Z_i. At this point, an isotropic and homogeneous spherical diffusion verifies, with respect to the mass centre. Therefore, if the time increases, particle's dispersion increases too, compared to the centre of mass in a homogeneous way.

An average particle's position could be expressed by an equation:

$$\langle Z \rangle = \frac{1}{N} \sum_N^1 Z_i \tag{4.7}$$

$$\sigma_z = \langle (Z - \langle Z \rangle)^2 \rangle \tag{4.8}$$

$$\sigma_z = \frac{1}{N} \sum_1^N (Z_i - \langle Z_i \rangle)^2 \qquad (4.9)$$

N is the number of particles involved.

For time high enough ($t > 10\ T_L$):

$$\langle Z \rangle = V_s\ t \qquad (4.10)$$

$$\sigma^2 \approx 2\ D_t\ t \qquad (4.11)$$

where D_t is the particles' dispersion coefficient, and $\sigma_X^2/(\sigma_U^2\ T_L)$ explains how standard deviation changes in time, considering that particles disperse themselves in the fluid, during the time (t), in homogeneous directions respect to the centre of mass, as shown in Fig. 32.
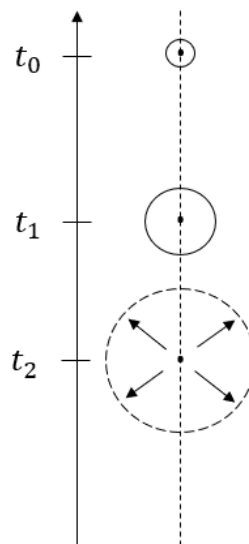
Fig. 32 – Dispersion of the particle respect to centre of mass in time.

The possible statistical motion of all the particles considered is reported in Fig. 33.
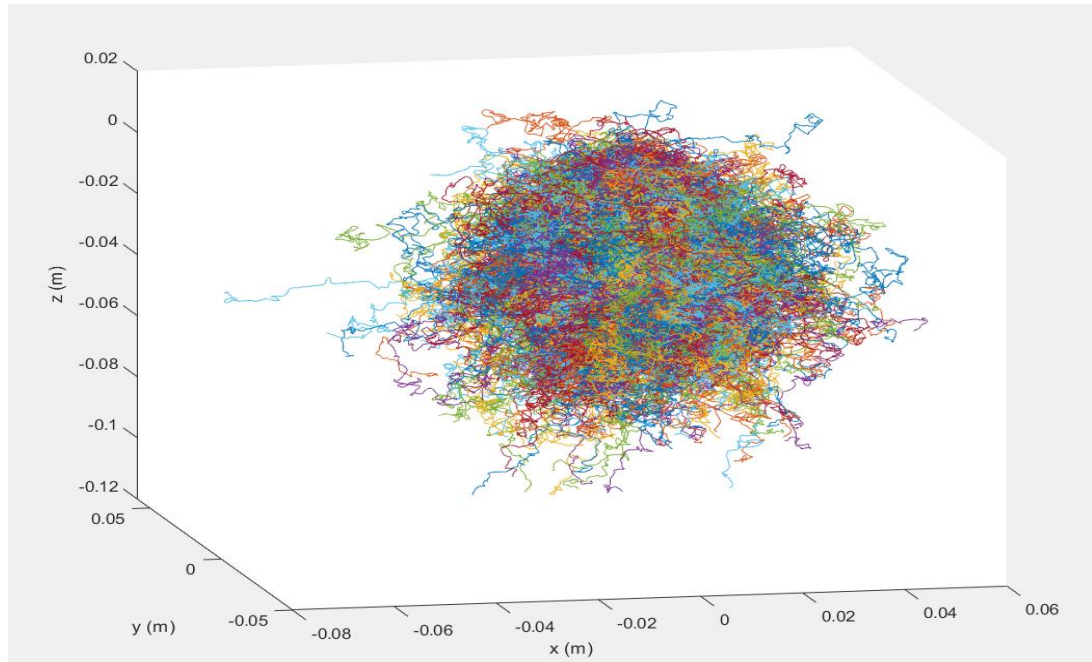
Fig. 33 – Random movement of single particles in free-stream turbulence.

Comparison of the cases of study

Comparison between results obtained from the two cases is plotted and reported in Fig. 34.
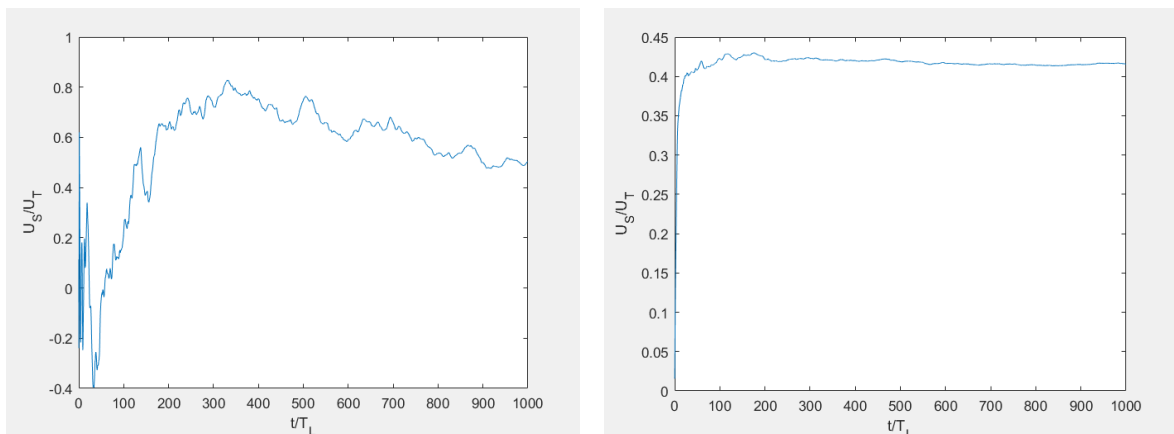
Fig. 34 – Comparison between the ratio between settling velocity and that in the still fluid in the two different cases of study.

Since second's case curve tends to an asymptotic value, giving the possibility to extrapolate a single constant value, an accurate estimation of the ratio of velocities could be reached. This tendency occurs because a greater number of particles provide a better statistical analysis.

Also, the particle's statistical settling among z-axis versus time has been compared (Fig. 35).
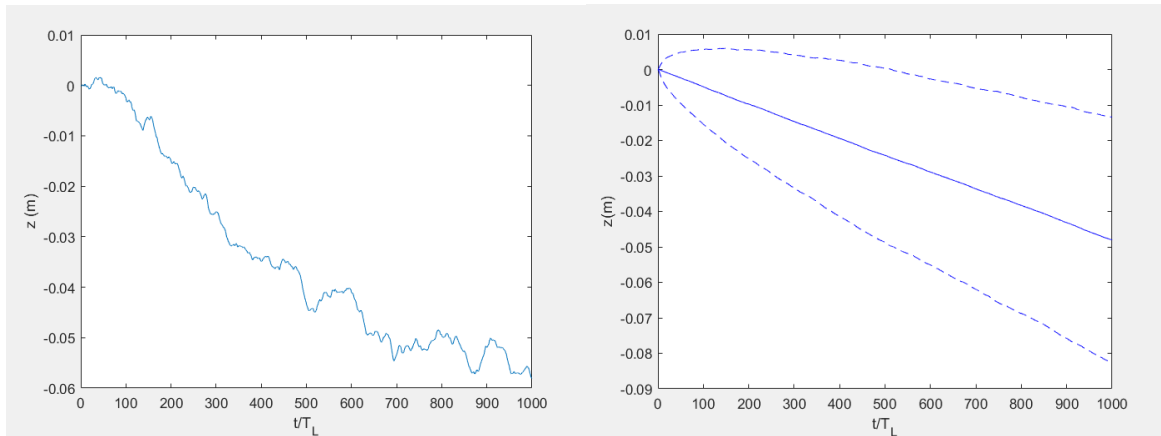
Fig. 35 – Plot of the statistical altitude change over time in the two different cases of study.

The second case of study allows predicting a more realistic field of motion. In fact, the right plot shows a $+/-$ two times value, figured by dashed lines, and an average value. Therefore, simulation involving a single particle doesn't allow to accurately predict the field of motion, because another realisation would have a completely different trajectory.

Once, it can be understood that increasing the particles' number lead to improve the description of their statistical behaviour. Thus, by considering the same characteristics stated before, one can conduct further simulations, by also acting on a time interval (T_L/N_t). Settling velocity and diffusion coefficient are evaluated (Table 6).

Np	$T_L/10$	$T_L/20$	$T_L/50$
1000	$V_s = 0,4190$ $D_t = 7,036 \times 10^{-5}$	$V_s = 0,4179$ $D_t = 7,4671 \times 10^{-5}$	$V_s = 0,4196$ $D_t = 7.2236 \times 10^{-5}$
2000	$V_s = 0,4129$ $D_t = 7,3305 \times 10^{-5}$	$V_s = 0,4238$ $D_t = 7,2503 \times 10^{-5}$	$V_s = 0,4232$ $D_t = 7.3740 \times 10^{-5}$
5000	$V_s = 0,4206$ $D_t = 7.1482 \times 10^{-5}$	$V_s = 0,4195;$ $D_t = 7.4529 \times 10^{-5}$	$V_s = 0,4228$ $D_t = 7,4055 \times 10^{-5}$

Table 6 – Simulation of the number of particles against time interval for diffusivity and settling velocity.

Results suggest that by decreasing the interval time and increasing the number of the particles asymptotic values for V_s and D_t maybe reached.

In this work, one thousand particles and an interval time equal to $T_L/100$ have been used to manage results; another increase of these parameters would require more time for simulations. This choice does not introduce any further significant increase in the final percentage error.

Chapter V − Correlation Proposed

The scope of this thesis is to propose a correlation able to describe particles' settling velocity immersed in a turbulent fluid.

The starting point is calling into question dimensionless parameters proposed by Spelt and Biesheuvel (1994), Brucato et al. (1998), Lane et al. (2007) and Magelli et al. (2008) discussed in Chapter I and respectively reported below.

$$\beta = \frac{u_0}{V_T}$$

$$\frac{\lambda}{d_p}$$

$$St = \frac{\tau_p}{T_L}$$

$$R_i = \frac{g \, \Delta\rho \, L}{\rho_f \, u_0{}^2}$$

$$\left(\frac{\rho_s - \rho_f}{\rho_f}\right)$$

Thus, following their suggestion, settling velocity is a function of those parameters:

$$Us = f\ (U_t, \rho_s, \rho_f, d_p, g, T_L, u_0) \tag{5.1}$$

The correlation has been written by using the Buckingham theorem (see Appendix I), and thanks to dimensional analysis, a single equation in which dimensionless terms appear has been proposed.

$$\frac{U_s}{Ut} = f\ \left(\frac{d_p}{\sigma\, T_L}, \frac{\sigma}{U_t}, \frac{\Delta\rho}{\rho_f}, \frac{t_r}{T_L}, \frac{g\, \Delta\rho\, L}{\rho_f\, \sigma}\right) \tag{2.1}$$

$$\frac{Us}{Ut} = f\ (\Psi1, \Psi2, \Psi3, \Psi4, \Psi5) \tag{5.2}$$

Where:

$\Psi 1 = \dfrac{d_p}{\sigma\, T_L}$, with $\sigma\, T_L = L$, where L is the Integral length scale.

Many different assets have been tested by varying ρ_s, ρ_f, d_p, μ, and $k,\ \varepsilon$, according to Langevin equation (Eq. 3.2.25).

k	ε	d_p	ρ_s	ρ_f	μ
$0,08 \div 0.2$	$2 \div 15$	$2,5 \times 10^{-4}$ $\div 3,5 \times 10^{-3}$	$1200 \div 4000$	$600 \div 1500$	5×10^{-4} $\div 5 \times 10^{-3}$

Table 7 – Range of parameter considered for correlation proposed.

All parameters are considered in S.I units.

Correlation proposed is:

$$\frac{Us}{Ut} = a \left(\frac{dp}{L}\right)^{b} \left(\frac{\sigma}{V_T}\right)^{c} \left(\frac{\Delta\rho}{\rho_f}\right)^{d} \left(\frac{t_r}{T_L}\right)^{e} \left(\frac{g\,\Delta\rho\,L}{\rho_f\,\sigma}\right)^{f} \qquad (5.3)$$

Constant values *a, b, c, d, e, f* have been evaluated by tending to zero the root mean square of deviation between experimentally-obtained values of settling and terminal velocities ratio against those deriving from correlation (Eq.(5.3)).
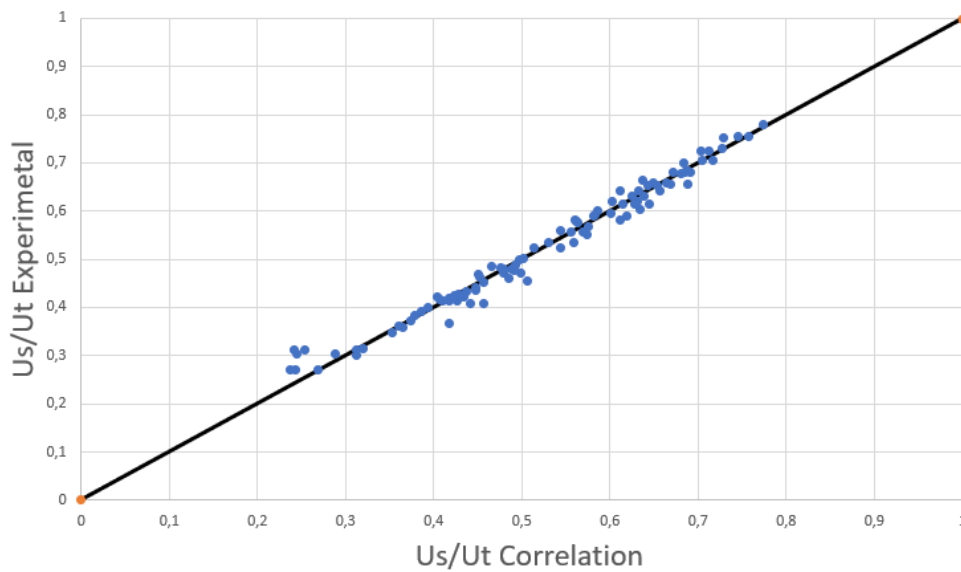
Fig. 39 – Plot where experimental values of Us/U_t have been compared with Us/U_t values from correlation.

Experimental points obtained have been fitted linearly, as it can be seen from Fig.39.

The correlation proposed explains solid particles' settling velocity in turbulent flows, with a determination coefficient $R^2 = 0{,}979$.

Finally, constants have been determined:

R^2	a	b	c	d	e	f
0,979	0,812	0,248	−0,007	0,201	−0,142	0,089

Table 8 – Constants' values of the proposed correlation and determination coefficient R^2.

therefore, Eq.(5.3) becomes:

$$\frac{Us}{Ut} = 0{,}812 \left(\frac{dp}{L}\right)^{0{,}248} \left(\frac{\sigma}{U_t}\right)^{-0{,}007} \left(\frac{\Delta\rho}{\rho}\right)^{0{,}201} \left(\frac{t_r}{T_L}\right)^{-0{,}142} \left(\frac{g\,\Delta\rho\,L}{\rho_f\,\sigma}\right)^{0{,}089} \qquad (5.4)$$

Chapter VI − Conclusions

The aim of this thesis' work is to propose an effective correlation to express particles' settling velocity immersed in a turbulent fluid, conducting simulations on MATLAB^{TM} programming software.

Several literature studies have been analysed, extrapolating dimensionless groups from Spelt and Biesheuvel (1997), Brucato et al. (1998), Lane et al. (2007) and Magelli et al. (2008) that well fit in the correlation proposed.

Langevin equation has been used in defining fluid's flow in homogeneous isotropic turbulence and deployed on programming software by Runge-Kutta method.

The trajectory's simulations of inertial particles have been performed with some assumptions, a forces' balance has been used, without involving Basset force, that is not easy to implement numerally and has a limited impact on particle's kinematics.

Furthermore, interactions between particles have not considered. As they might cause changes in their trajectory, consistency of data.

A system composed of a fluid-filled with 1000 particles has been studied, considering adding them once per time. The software has been able to develop an average settling velocity value; this implies errors, due to the limited nature of the simulations carried out, even if small.

In order to prove the correlation's reliability, values of the ratio between particles settling velocity and that in still fluid have been compared with results of simulations.

In conclusion, the comparison confirmed that data provided by correlation, fit the simulation's data, on the range of physical properties of fluid and particles considered.

Chapter VII – Future Work

Further studies may be conducted starting from this thesis work, by improving the proposed correlation.

In this work, one thousand particles have been performed with an interval time equal to $T_L/100$ and observation time of $max(1000 \cdot T_L, 50 \cdot t_r)$; to explore other assets, one could increase particles' number involved, and the observation time as well, by decreasing amplitude of intervals time, simultaneously.

Obviously, complicating simulation means longer time in obtaining results.

In order to verify data truthfulness, they would have compared with those deriving from laboratory experiments.

In conclusion, new studies and experiments may be carried out aiming to outline parameters which affect settling phenomenon.

Appendix

Buckingham theorem

The Buckingham theorem is based on the assumption that the relations used are dimensionally homogeneous, or that all the terms of an equation have the same dimensions.

If this hypothesis is verified we can affirm that if a phenomenon is governed by N parameters through a relation of the type $f(P1, P2, \ldots, PN) = 0$, and these N parameters can be described by K fundamental dimensions (K minimum number), it is then possible to study the phenomenon through $N - K$ dimensionless groups Ψi with a type relationship $g(\Psi 1, \Psi 2, \ldots, \Psi N - K) = 0$.

To pass from the function f to the function g we must identify a base of K variables Pi that are used to render the remainder unbalanced and the variable K must have the following characteristics:

1. Contain all the basic K dimensions.

2. They are independent of each other, that is, they must not by themselves constitute a dimensionless group.

Simulation Code

Sdesys Function

```
function [tp,yp] = sdesys(a,b,tspan,y0,h,varargin)

if nargin<4
error('at least 4 input arguments required')
end
if any(diff(tspan)<=0)
error('tspan not ascending order')
end
n = length(tspan);
ti = tspan(1);
tf = tspan(n);
if n == 2
t = (ti:h:tf)';
n = length(t);
if t(n)<tf
t(n+1) = tf;
n = n+1;
end
else
t = tspan;
end

tt = ti;
y(1,:) = y0;
np = 1;
tp(np) = tt;
yp(np,:) = y(1,:);
i=1;

while(1)
tend = t(np+1);
hh = t(np+1) - t(np);

if hh>h
hh = h;
end
while(1)
```

- if tt+hh>tend
    o hh = tend-tt;
- end

- dW=randn(1,length(y0))*sqrt(hh);
- S=(-1)^randi([0 1]);

- k1 = hh*a(tt,y(i,:),varargin{:})'+(dW-S*sqrt(hh)).*b(tt,y(i,:),varargin{:})';
- k2 = hh*a(tt+hh,y(i,:)+k1,varargin{:})'+(dW+S*sqrt(hh)).*b(tt+hh,y(i,:)+k1,varargin{:})';

- y(i+1,:) = y(i,:) + 1/2*(k1+k2);

- tt = tt+hh;
- i=i+1;
- if tt>=tend
- break
- end
- end
- np = np+1;
- tp(np) = tt;
- yp(np,:) = y(i,:);
- if tt>=tf
- break
- end
- end

Test Code

```
tic

k=0.1;
epsilon=10;

g=[0,0,-9.81];
mu=1e-3;
dp=.5e-3;
rhop=2000;
rhof=1000;

sigma=sqrt(2/3*k);
ReT=sqrt(15*sigma/(epsilon*mu/rhof));
C0=6.5/(1+140*ReT^(-4/3))^(3/4);
TL=1/(3/4*C0*epsilon/k);

vterm=-fzero(@(x) x^2-4/3*(rhop-rhof)/rhof*dp*9.81./cdsn(rhof*dp*x/mu),[0 100]);

tr=(rhop/rhof+0.5)*dp/(3/4*cdsn(rhof*dp*abs(vterm)/mu)*abs(vterm));

%tspan=[0 max(1000*TL,50*tr)];
tspan=[0 1000*TL];
y0=zeros(9,1);
h=TL/100;

np=1000; % Number of particles

%parfor i=1:np
for i=1:np
[tp(:,i),ypart(:,:,i)] = sdesys(@a,@b,tspan,y0,h,TL,sigma,mu,dp,rhop,rhof,g);

end

tp=tp(:,1)';
yp=mean(ypart,3);

figure(1)
plot(tp/TL,yp(:,9)'./tp/vterm)
xlabel('t/T_L')
ylabel('U_S/U_T')
```

- usut=yp(length(tp),9)/tp(end)/vterm;
- DT=var(ypart(length(tp),9,:),1,3)/(2*tp(end));

- lambdaK=((mu/rhof)^3/epsilon)^.25;

- lambdadp=logspace(-4,0,100);
- % New Correlation (2019)
- usutE=((0.32*tanh(sqrt((rhop-rhof)/rhof)*19*lambdadp-1)+0.6))*(tr/TL);
- % Brucato et al. (1998)
- usutB=((1+8.76e-4*lambdadp.^(-3)).^(-0.5))*(tr/TL);

- figure(2)
- semilogx(lambdaK/dp*sqrt((rhop-rhof)/rhof),usut,'ok',lambdadp*sqrt((rhop-rhof)/rhof),usutE,'--r',lambdadp*sqrt((rhop-rhof)/rhof),usutB,'--g')
- axis([0.001,1,0,1])
- xlabel('\lambda/d_p (\Delta\rho/\rho_f)^{0.5}')
- ylabel('U_S/U_T')

- figure(3)
- loglog((dp./lambdaK).^3,usut.^(-2)-1,'ok',lambdadp.^(-3),usutF.^(-2)-1,'--r',lambdadp.^(-3),usutB.^(-2)-1,'--g')
- axis([1,1e6,0.01,100])
- xlabel('(d_p/\lambda)^{3}')
- ylabel('(C_D-C_{D0})/C_{D0}')

- figure(4)
- plot(tp/TL,yp(:,9),'b-',tp/TL,yp(:,9)+2*std(ypart(:,9,:),1,3),'b--',tp/TL,yp(:,9)-2*std(ypart(:,9,:),1,3),'b--')
- xlabel('t/T_L')
- ylabel('z(m)')

- figure(5)
- loglog(tp/TL,var(ypart(:,7,:),1,3)/(sigma^2*TL),tp/TL,var(ypart(:,8,:),1,3)/(sigma^2*TL),tp/TL,var(ypart(:,9,:),1,3)/(sigma^2*TL))
- xlabel('t/T_L')
- ylabel('\sigma^2_X/(\sigma^2_U T_L)')

- figure(6)
- loglog(tp/TL,abs(yp(:,9))/(sigma*TL))
- xlabel('t/T_L')
- ylabel('|z(m)|/(\sigma_U T_L)')

- for i=1:np

- figure(6)
- hold on

- plot(tp/TL,ypart(:,9,i))
- xlabel('t/T_L')
- ylabel('z (m)')
- hold off

- figure(7)
- hold on
- plot3(ypart(:,7,i),ypart(:,8,i),ypart(:,9,i))
- xlabel('x (m)')
- ylabel('y (m)')
- zlabel('z (m)')
- hold off

- end

- toc

- function dydt = a(t,y,TL,sigma,mu,dp,rhop,rhof,g)

- umag=sqrt((y(1)-y(4))^2+(y(2)-y(5))^2+(y(3)-y(6))^2);
- re=rhof*dp*umag/mu;

- dydt(1) = -y(1)/TL;
- dydt(2) = -y(2)/TL;
- dydt(3) = -y(3)/TL;
- dydt(4) = 3/4*cdsn(re)/dp*rhof/(rhop+.5*rhof)*abs(y(1)-y(4))*(y(1)-y(4))+rhof/(2*(rhop+.5*rhof))*dydt(1)+(rhop-rhof)/(rhop+.5*rhof)*g(1);
- dydt(5) = 3/4*cdsn(re)/dp*rhof/(rhop+.5*rhof)*abs(y(2)-y(5))*(y(2)-y(5))+rhof/(2*(rhop+.5*rhof))*dydt(2)+(rhop-rhof)/(rhop+.5*rhof)*g(2);
- dydt(6) = 3/4*cdsn(re)/dp*rhof/(rhop+.5*rhof)*abs(y(3)-y(6))*(y(3)-y(6))+rhof/(2*(rhop+.5*rhof))*dydt(3)+(rhop-rhof)/(rhop+.5*rhof)*g(3);
- dydt(7) = y(4);
- dydt(8) = y(5);
- dydt(9) = y(6);

- dydt=dydt';
- end

- function dydt = b(t,y,TL,sigma,mu,dp,rhop,rhof,g)
- dydt(1) = sqrt((2*sigma^2)/TL);
- dydt(2) = sqrt((2*sigma^2)/TL);
- dydt(3) = sqrt((2*sigma^2)/TL);
- dydt(4) = rhof/(2*(rhop+.5*rhof))*dydt(1);
- dydt(5) = rhof/(2*(rhop+.5*rhof))*dydt(2);
- dydt(6) = rhof/(2*(rhop+.5*rhof))*dydt(3);
- dydt(7) = 0;

- dydt(8) = 0;
- dydt(9) = 0;

- dydt=dydt';
- end

- function cd=cdsn(re)
- if re<=1000
- cd=24./(re+1e-20).*(1+0.15*re.^0.687);
- else
- cd=0.44;
- end
- end

Figure Index

Bibliography

[1]   Bec J., Homann H., Ray S. S., Gravity-Driven Enhancement of Heavy Particle Clustering in Turbulent Flow, Phys. Rev. Lett. 112 (18), 1–5 (2014)

[2]   Biesheuvel A. and Spelt P. D. M., On the Motion of Gas Bubbles in Homogeneous Isotropic Turbulence, J. Fluid Mech., vol. 336 pp. 221-244, (1997)

[3]   Brucato A., Grisafi F., Montante G., Particle Drag Coefficients in Turbulent Fluids, Chem. Eng. Sci. Vol.53, No.18, (1998)

[4]   Cheng N. S. and Zhou Q., Experimental Investigation of Single Particle Settling in Turbulence Generated by Oscillating Grid, Chem. Eng. J. 149 (1-3), 289–300 (2009)

[5]   Doran Pauline M., Fluid Flow, Bioprocess Engineering Principles (Second Edition), (2013)

[6]   Doroodchi E., Evans G.M., Lane G.L., Schwarz M.P., Shan N., A. Nguyen, Influence of Turbulence Intensity on Particle Drag Coefficients, Chemical Engineering Journal 135 129-134, (2008)

[7]   Evans G.M., Lane G.L., Schwarz M.P., Numerical Modelling of Gas-Liquid Flow in Stirred Tanks, Chem. Eng. Sci. 60 2203-2214, (2005)

[8]   Fajner D., Ghadge R.S., Magelli F., Montante G., Paglianti A., Pinelli D., Solids Distribution and Rising Velocity of Buoyant Solid Particles in a Vessel Stirred with Multiple Impellers, Chemical Engineering Science 63, 5876-5882 (2008)

[9]   La Rocca M., Dispense del Corso di Modelli di Trasporto Turbolento

[10]   Lam K. M., Lu Y., Wang Y., Settling Velocity of Fine Heavy Particles in Turbulent Open Channel Flow, Physics of Fluids 30, (2018)

[11]   Lei U. and Yang C. Y., The Role of The Turbulent Scales in The Settling Velocity of Heavy Particles in Homogeneous Isotropic Turbulence, J. Fluid Mech. 371, 179–205 (1998)

[12]   Maxey M. R and Wang L.P., Settling Velocity and Concentration Distribution of Heavy Particles in Homogeneous Isotropic Turbulence, J. Fluid Mech. 256, 27–68 (1993)

[13]   Magelli F., Montante G., Paglianti A., Particle Settling Velocity in Slurry Stirred Vassels, 16th Int Symp on Application of Laser Techniques to Fluid Mechanicals, Lisbon, Portugal, (2012)

[14]   Montante G., Modelling and Simulations of Single-Phase and Solid-Liquid Stirred Vessels, PhD Thesis, Università di Palermo, (2000)

[15]   Pope Stephen B., Turbulent flow, (2000)

[16]   Pope Stephen B, Simple Models of Turbulent Flows, Physics of Fluids 23, (2011)

[17]   Verzicco R., Appunti Turbolenza, (2007)

Web Site

[18]   Le Scale della Turbolenza, http://www.arpalazio.net, (2010)